ISSN 0973-3302

THE JOURNAL OF ACOUSTICAL SOCIETY OF INDIA

Volume 45 Number 3 July 2018

A Quarterly Publication of the ASI
http://www.acousticsindia.org

The Journal of Acoustical Society of India

Volume 45 Number 3 July 2018 pp 111-164

The Journal of Acoustical Society of India

The Refereed Journal of the Acoustical Society of India (JASI)

The Journal of Acoustical Society of India is a refereed journal of the Acoustical Society of India **(ASI)**. The **ASI** is a non-profit national society founded in 31st July, 1971. The primary objective of the society is to advance the science of acoustics by creating an organization that is responsive to the needs of scientists and engineers concerned with acoustics problems all around the world.

Manuscripts of articles, technical notes and letter to the editor should be submitted to the Chief Editor. Copies of articles on specific topics listed above should also be submitted to the respective Associate Scientific Editor. Manuscripts are refereed by at least two referees and are reviewed by Publication Committee (all editors) before acceptance. On acceptance, revised articles with the text and figures scanned as separate files on a diskette should be submitted to the Editor by express mail. Manuscripts of articles must be prepared in strict accordance with the author instructions.

All information concerning subscription, new books, journals, conferences, etc. should be submitted to Chief Editor:

B. Chakraborty, CSIR - National Institute of Oceanography, Dona Paula, Goa-403 004,
Tel: +91.832.2450.318, Fax: +91.832.2450.602, e-mail: bishwajit@nio.org

Annual subscription price including mail postage is Rs. 2500/= for institutions, companies and libraries and Rs. 2500/= for individuals who are not **ASI** members. The Journal of Acoustical Society of India will be sent to **ASI** members free of any extra charge. Requests for specimen copies and claims for missing issues as well as address changes should be sent to the Editorial Office:

ASI Secretariat, C/o Acoustics, Ultrasonics & Vibration Section, CSIR-National Physical Laboratory, Dr. KS Krishnan Road, New Delhi 110 012, Tel: +91.11.4560.8317, Fax: +91.11.4560.9310, e-mail: asisecretariat.india@gmail.com

ISSN 0973-3302

Printed at Alpha Printers, WZ-35/C, Naraina, Near Ring Road, New Delhi-110028 Tel.: 9810804196. JASI is sent to ASI members free of charge.

ASI

The Journal of Acoustical Society of India

A quarterly publication of the Acoustical Society of India

Volume 45, Number 3, July 2018

ARTICLES

INFORMATION

PREFACE

Journal of Acoustic Society of India (JASI), has been publishing quality research papers and the ~~state of art of the art~~ research findings from this region. It also covers publication of articles on specific problems which is relevant to underwater acoustics, instrumentation and technological advances. The special issue on ***"Design of a High-resolution Sub-bottom Profiling Sonar "*** (HSPS)" is a compilation of insightful papers that addresses acoustic imaging and communications research. The publication will provide a wide scope of the assessment of Indigenous research and development within the country specific to acoustic imaging program. The special issue highlights six papers that were peer-reviewed and accepted out of ten solicited manuscripts. A portable tow based sonar system for operation in shallow waters has been designed and achieved with a compact FPGA based instrumentation. This has realized a prototype active buried object detection sonar which has a potential spin-off for ~~the~~ further improving it as a shallow water sub-bottom profiler. Overall system architecture is described by Sreedev *et al.* The FPGA based design can handle the simultaneous acquisition of data using a multichannel (32 element) hydrophone array with time synchronization. It is good to be adopted for any laptop based active sonar system in the future. In addition to acoustic data, the sonar has DGPS and motion sensor for position, pitch and roll measurements. The tow body sub-systems are connected to the deck signal processing unit (In a boat or ship) through an umbilical power and a Kevlar cable. Development of software and its integration with the hardware is also accomplished. A linear frequency modulated chirp signal in the frequency range (2 - 24kHz) is utilized and is detailed by Sayanti et al. Chithra et al has presented the performance analysis of coding techniques in underwater acoustic communication were an acoustic modem was developed for operation up to 1100 meter water depths using orthogonal frequency division, multiplexing (OFDM) scheme. The target detection using artificial bee colony based TSALLIS entropy is briefed by Rajeshwari *et al.* The indigenous prototype sub-bottom profiler could penetrate up to 9 meters in clay and 1 - 2 meters in mixed sand sediments. Detection of different types of objects like concrete blocks, metal plates, naturally buried stones and proud objects projecting from the seabed as well as a sub-bottom profiler showing multi seabed layers have also been detected with the system.

The guest editor thanks Dr. M.A. Atmanand, Director, National Institute of Ocean Technology for permitting the work to be published in the special issue. Special thanks are due to Chief Editor, JASI, Dr. Bishwajit Chakraborty, (CSIR-NIO, Goa) and Dr. Monika Aggarwal, IIT, Delhi for the critical review of the papers who have made the manuscripts for publication . The special issue could not have been realized without the whole hearted co-operation and support from the team members of Marine Sensor Systems. Grateful to my senior colleagues at NIOT, Dr. G. Latha, Tata Sudhakar and Dr. G.A. Ramadass. I acknowledge help from Dr. Bishwajit Chakraborty, Chief Editor to bring out this special issue.

Dr. Dhilsha Rajapan
Guest Editor

The Journal of Acoustical Society of India : Vol. 45, No. 3, 2018 (pp. 111-120)

Compact FPGA based instrumentation for a buried object detection sonar

D.S. Sreedev, Dhilsha Rajapan, Shibu Jacob, Shijo Zacharia, K Arumugam, P.M. Rajeshwari and M.A. Atmanand
National Institute of Ocean Technology (NIOT), Chennai, India 600100
sreedev@niot.res.in

[Received: 20-09-2017; Revised: 15-04-2018; Accepted: 10-05-2018]

ABSTRACT

One of the major requirements in active sonar is precise time synchronized ping generations and acquisition of corresponding backscatter data. Also the backscatter data corresponding to each ping should be geo referenced. Design and generation of a suitable transmitting waveform with windowing is also important for sonars which are meant for detecting objects buried under sea bed. This paper details an FPGA based instrumentation scheme developed for the realization of active buried object detection sonar developed in National Institute of Ocean Technology (NIOT) [1], [2], [3], Chennai. The FPGA based design to handle concurrent events with time synchronization is the major highlight of the paper, which could be adapted for any active sonar systems.

1. INTRODUCTION

The buried object detection sonar[4],[5],[6] is active sonar in which an acoustic projector illuminates the sea bed to be imaged. A receiver array comprises of a number of hydrophone elements collects the backscatter data. Change in acoustic impedance in sea bed layers and buried objects, results in signal reflections. Beam forming the received signal and match filtering with the transmitted signal, results in waveform with multiple peaks[7],[8]. Each peak corresponds to reflections from successive layers and buried objects in sea bed. The time difference between each successive peak corresponds to the spatial separation between successive layers and buried objects in sea bed.

Since its active sonar, signal transmission and acquisition of backscatter data to be synchronized. Transmitting signal is to be generated with pre defined frequency range, pulse width, amplitude, *etc.* Also, the transmitting signal generation is to be repeated at a pre- determined time interval, which is calculated as per the to and fro travel time required for the acoustic pulse for the specified range of the sonar. So a number of signal generations (pings) to made in every second, as per the range. After each ping generation, data to be acquired for predefined time duration. In shallow waters, to avoid unwanted multiple reflections, the data acquisition duration after each ping generation to be limited as per the depth of operation of the sonar. In order to implement array signal processing algorithms like beam forming, data to be collected from all the hydrophone elements simultaneously. For this, precise time synchronized simultaneous sampling to be done at the hydrophone outputs. The ping generations and data acquisition to be time synchronized for accurate range estimates. Also for better SNR, the hydrophones outputs are to be sampled as close the array as possible.

In addition to acoustic data, sonar has to acquire data from GPS and motion sensor for position, pitch and roll measurements. Each ping to be geo referenced with the data from GPS. Also, the data acquired from the hydrophone arrays, to be transferred before the next ping generation, to the signal processing unit, for real time processing and image generation. Hardware architecture of a 252 channel sonar system is described in[9], where a multiplexer is used to combine the channels. But the use of multiplexer will affect simultaneous sampling requirements. Design of a custom built chip for a high resolution sonar array is described in[10], but it's not commercially available. Since off the shelf systems are not meeting the above all requirements, a custom built system is designed and developed. The issues described above are addressed with a Field Programmable Gate Array (FPGA) based instrumentation scheme detailed in subsequent sections. The system is designed around FPGA for handling concurrent operations. The indigenous design helped to maintain better time synchronization among different events with a common clock. The overall architecture and the system design to handle concurrent events with time synchronization could be adapted for any active sonar design requirements.

2. SYSTEM ARCHITECTURE

In the buried object detection sonar, the transducer, hydrophone arrays and electronic subsystems are in a tow body and sonar signal processor with Graphical User Interface (GUI) is on deck. The tow body subsystems are connected to the deck side signal processing unit through an umbilical power and signal Kevlar cable as shown in Fig 1. The signal interface is 10/100 Mbps Ethernet.

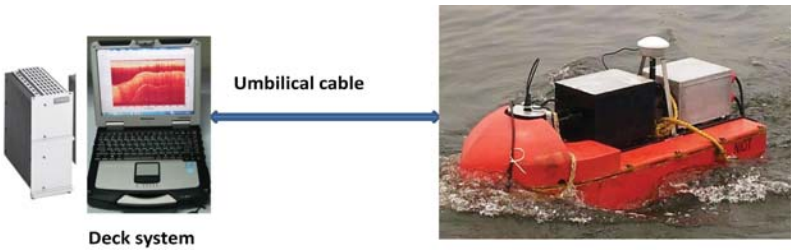

Fig. 1. Dry and wet end systems of the sonar

The overall system architecture is shown in Fig 2. The tow body consists of subsystems for acoustic signal generation, back scatter data acquisition and data streaming to deck side signal processing unit.

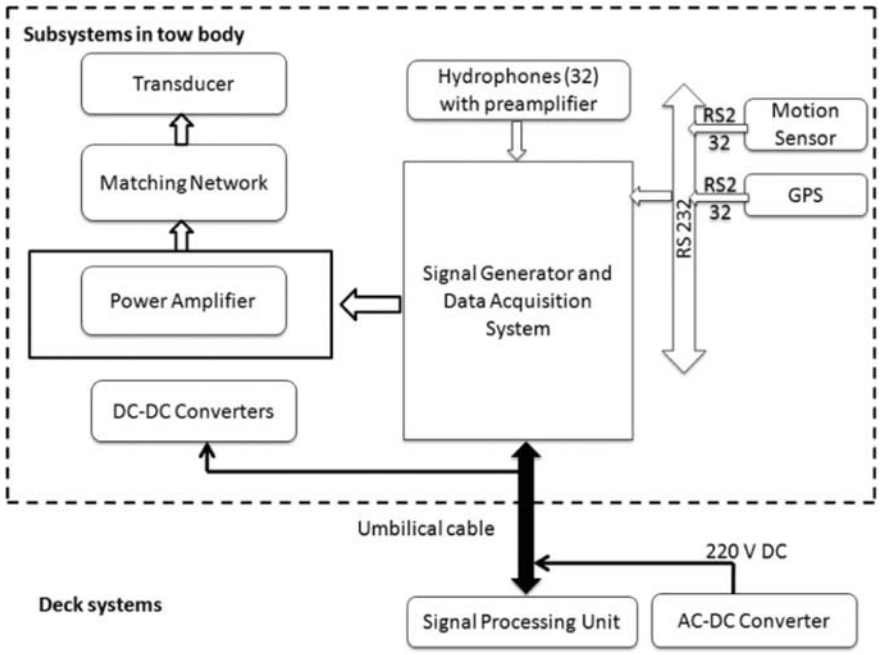

Fig. 2. Overall system architecture of buried object detection sonar

FPGA based instrumentation is devised in the tow body for sonar signal generation, acquisition and streaming to deck side signal processing unit. The heart of the system is an FPGA based signal generator and data acquisition system, which generates the signal to be transmitted, acquires data from hydrophone arrays and streams the digitized data to the deck in real time.

2.1 FPGA based instrumentation in tow body

The hardware architecture of the system in tow body for sonar signal generation, acquisition and streaming is shown in Fig 3. The system is designed around FPGA which generates the control and timing signals for the entire operations. A 100 MHz clock is used to maintain timing requirements. The system can be divided into two sections; namely, signal generator section, data acquisition and streaming section. The system is designed in such a way that sonar operational parameters are configurable in FPGA through a GUI in deck. User Datagram Protocol (UDP) is chosen as the communication protocol between FPGA and deck end GUI. To store the sonar operational parameters, variables are created in the FPGA, which are configurable during initialization through UDP packets from the deck end GUI. UDPs with six different headers are used for communication between FPGA and deck end GUI. The payload for each type of UDP is shown in Table 1. The sonar operational parameters configurable in FPGA are shown in Table 2.

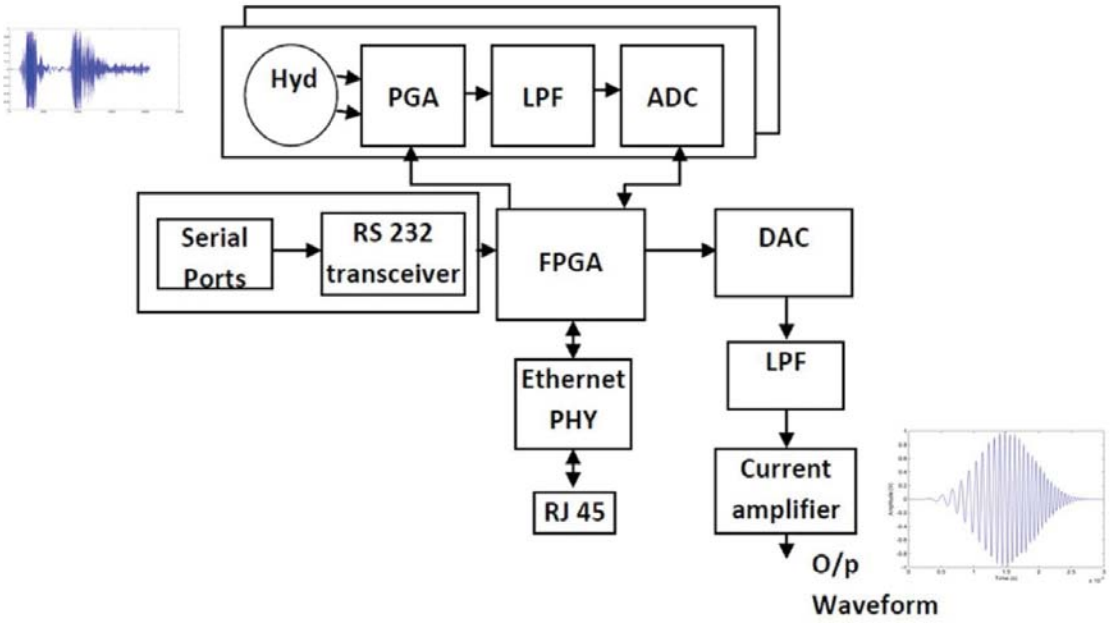

Fig. 3. FPGA based instrumentation in the tow body

Table 1. Type of UDP packets used for communication

Sl No.	Type of UDPs	Payload
1	UDP with header I	Wave form values to be send from GUI to FPGA
2	UDP with header II	Sonar operational parameters listed in Table 2
3	UDP with header III	Start command from GUI to FPGA for signal generation and acquisition operations
4	UDP with header IV	Digitized hydrophone data from FPGA to GUI
5	UDP with header V	Serial ports data from FPGA to GUI
6	UDP with header VI	Stop command from GUI to FPGA

Table 2. Sonar operational parameters configurable in FPGA

Sl No.	Sonar operational parameters	Values
1	Frequency	2-24 kHz
2	Pulse width	3-5 ms
3	Amplitude	1 to 10 Vpp
4	Number of pings/s	2-10
5	Data acquisition duration	10-50 ms
6	Programmable gain amplifier gains	0-60 dB

The transmitting waveform is created in deck in MATLAB and stores as a text file. The required pulse width, frequency and window of the wave form are decided while generating the waveform in MATLAB. Such a sample 3 ms waveform generated in MATLAB is shown in Fig 4, which is a chirp signal in 2-24 kHz bandwidth with Blackman-Harris window. Wide band chirp signal results in range resolution of the system in cm level[11]. In MATLAB, this 3 ms waveform is generated with 1 MHz sampling rate, which results 3000 values to represent the waveform. GUI transfers this text file to the FPGA, through UDP with header 1, during initial configuration.

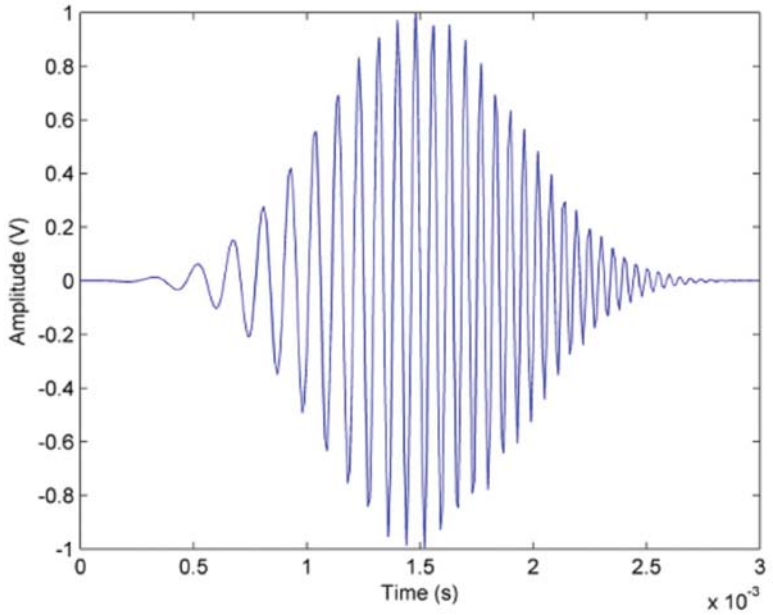

Fig. 4. Sample 3ms waveform generated in MATLAB in deck end

A 5000 element buffer is created in the FPGA to store the waveform values receive through UDP with header 1. The word size of each buffer element is 16 bits. FPGA writes the waveform values receive during initialization, through UDP with header 1, to these buffers. According to the pulse width (3-5 ms), the number of values to be written to the buffers varies from 3000-5000. Similarly, 2 byte buffers are created in FPGA to store each sonar operational parameters shown in Table 2. UDP with header II is used to transfer the sonar operational parameters to the FPGA. UDP with header III is a start command from deck end GUI to the FPGA for signal generation and acquisition.

Signal generator section is designed to generate chirp signal in the frequency range 2-24 kHz with 3-5 ms pulse width at a repetition rate of 2-10 signals per second. It is realized by interfacing a Digital to

Analog Converter (DAC) and an 8th order Butterworth low pass filter (LPF) followed by a current amplifier with the FPGA. The output of the current amplifier is fed to the acoustic transmitter through an acoustic power amplifier. The power amplifier raises the signal power to ~500 W. When FPGA receives UDP with header III (start command), it writes the waveform values stored in the waveform buffer to the buffer of the DAC, one by one, at a speed of 1 MHz. This results generation of a 3 ms pulse with required frequency and shape.

The system is designed to generate 2-10 pings/s as per user requirement. This corresponds to signal generation interval of 500 to 100 ms, which is maintained by creating a counter in the FPGA. Since the system clock is 100 MHz, the counter is initialized with values ranging from 5,00,00,000 to 1,00,00,000 as per the required pings/s. The end of each counting cycle generates a trigger signal, which initiates the transfer of waveform values from FPGA buffer to DAC buffer. At the end of the counting cycle, FPGA re-initializes the counter and the process repeats indefinitely till the stop command (UDP with header VI) receives from the deck.

At the receiver end, 32 channels are created where each channel has a dedicated Programmable Gain Amplifier (PGA) followed by an 8th order Butterworth low pass filter and an ADC. Since the frequency of operation of the sonar is 2-24 kHz, the sampling frequency is selected as 100 kHz with 16 bit resolution. To start acquisition, the trigger signal generated in the FPGA to maintain the required pings/s is used. This signal simultaneously triggers all ADCs, which ensures synchronization between signal generation and acquisition.

Another counter with a count value of 1000 is created in the FPGA to maintain the 100 kHz sampling rate. The counting operation is initiated with the trigger signal generated in the FPGA to maintain the required pings/s. End of the counting cycle generates another trigger signal. Since the system clock is 100 MHz, count value of 1000 results in generation of this trigger signal after 10 µs. This signal is used to further trigger all ADCs for simultaneous data acquisition. In order to maintain the 100 kHz sampling rate, FPGA re-initializes the counter after each counting cycle and the operation repeats for next 10 to 50 ms, as per acquisition duration communicated to the FPGA, through UDP with header II initially. Triggering at every 10 µs maintains the 100 kHz sampling rate.

UDP with header IV is used to transfer the digitized data from FPGA to deck end GUI. Since the UDP data packet size is 1500 bytes, 16 consecutive samples from all 32 channels, which sizes 1 KB, is used as a UDP data payload. FPGA sends the next 16 consecutive samples from all the channels in next UDP packet and the process continue till the specified data acquisition duration ends. Also during acquisition of each ping data, FPGA reads the data from two RS 232 serial ports corresponds to GPS and Motion sensor. FPGA sends the serial port data to the deck side GUI through UDP with header V. The above processes of data read and transfer from hydrophone array and serial ports repeats for the consecutive trigger signals from the FPGA.

To vary the gain, a Programmable Gain Amplifier (PGA) is incorporated in each acquisition channel, which has 2 bit gain control. This results in setting of four pre determined gains as per user requirement. FPGA sets the gain control bits as per the user input in UDP with header II. This has resulted in utilization of full dynamic range of the ADCs under different environmental conditions.

2.2 Software Architecture

The software architecture of the system in deck end GUI and FPGA are shown in Fig 5 and 6 respectively. After initial setup of sonar parameters in the GUI, a download command initiates sending of configuration UDP packets (UDP with header I and UDP with header II) to the signal generator and receiver board. Once the board is initialized, a start command (UDP with header III) from the GUI to the FPGA starts the signal generation and acquisition operations of the system as specified in the previous section. Once the system starts sending the digitized hydrophone and serial port data to the deck end, GUI receives each 1 KB sized UDP packets (UDP with header IV & UDP with header V) and de packetizes each. The data correspond to

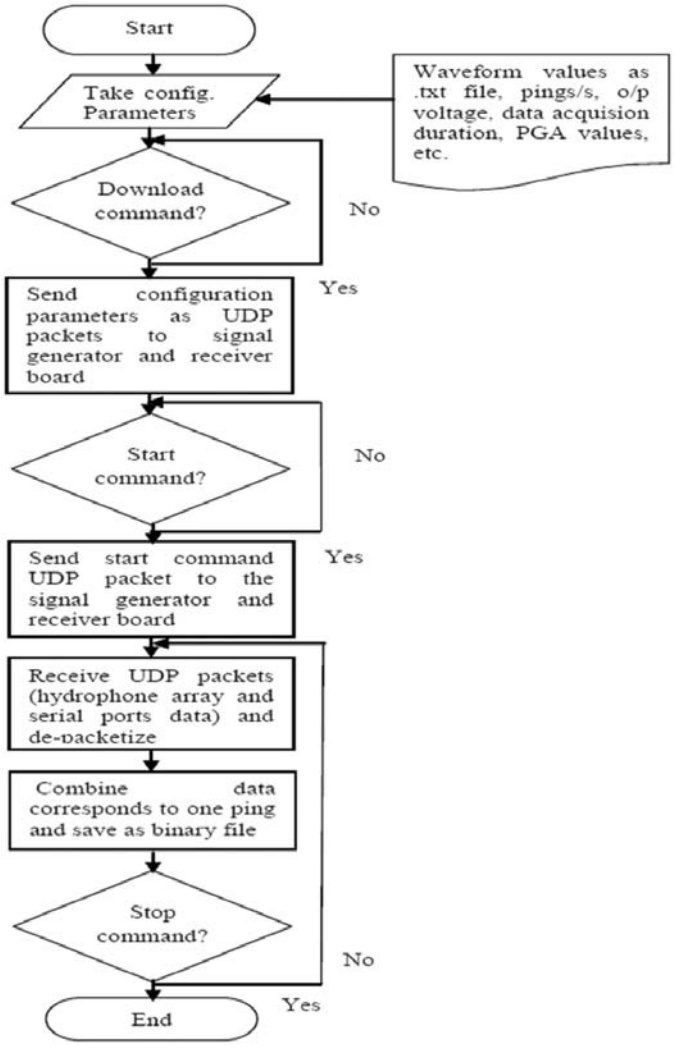

Fig. 5. Flow chart at GUI end

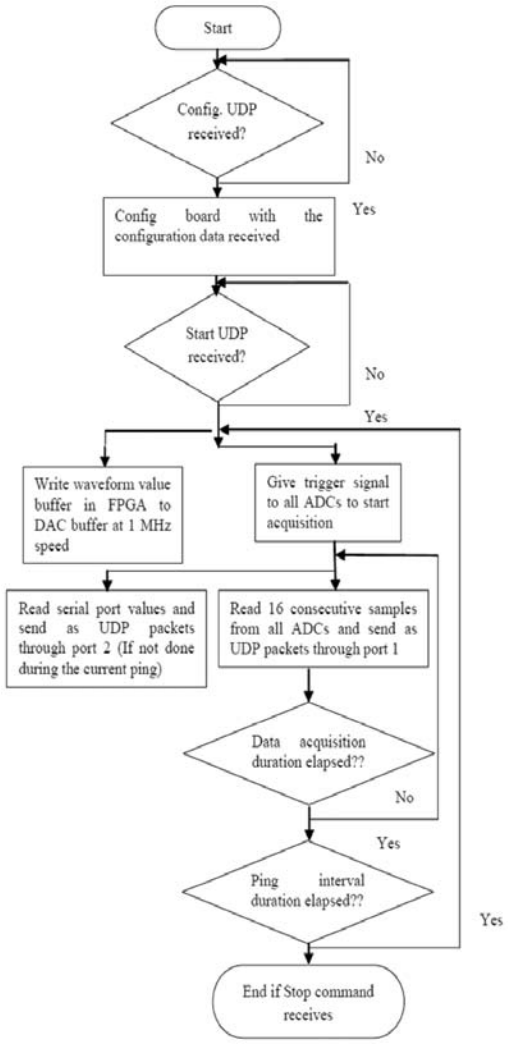

Fig. 6. Flow chart in FPGA

one ping is combined and passes to the signal processing module for real time signal processing and image generation. The process repeats indefinitely till FPGA receives the stop command (UDP with header VI) from deck by the user.

3. DATA SIZE CALCULATION

The signal acquisition duration is variable from 10 ms to 50 ms in discrete steps of 10 ms depends on the depth of operation of the sonar. 10 ms corresponds to the minimum acquisition duration required for 7.5 m water depth by considering the to and fro travel time of sound. Each 10 ms increase in acquisition duration results in increase in depth of operation from 7.5 m to 37.5 m. Since the sonar is designed for 30m water column depth operations, maximum acquisition duration is limited at 50 ms.

Table 3 shows the size of the received data corresponds to one ping for different depth of operations of the sonar. Data size/s Vs depth of operation of the sonar for different pings/s is shown in Fig 7. The maximum data size per second is 3.05 MB, which correspond to maximum designed pings/s, 10, and operational depth, 37.5 m, which is within the data rate limit of 10/100 Mbps Ethernet.

Table 3. Received data size corresponding to one ping for different depth of operations of the sonar

Water column depth (m)	Acquisition duration (ms)	Data packet size (KB)
7.5	10	62.5
15.0	20	125.0
22.5	30	187.5
30.0	40	250.0
37.5	50	312.5

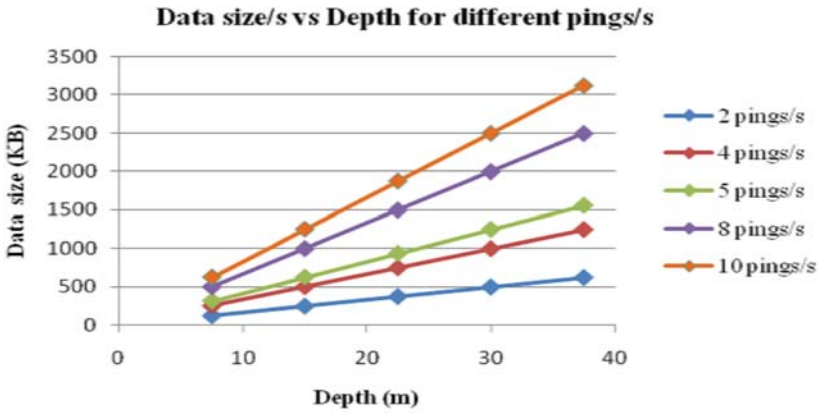

Fig. 7. Data size / s Vs Depth of operation for different pings / s

4. SYSTEM ASSEMBLY AND SEA TRIAL RESULTS

Major subsystems of the instrumentation setup in tow body for signal generation and acquisition are shown in Fig 8. The acoustic transmitter[12], hydrophone arrays[13], power amplifier, signal generator and receiver, GPS receiver and motion sensor are interfaced and assembled in two water tight enclosures as shown in Fig 9. The total system assembly in the tow body is shown in Fig 10.

Fig. 8. Major Subsystems in tow body

Fig. 9. System assembly in enclosures

Fig. 10. System assembly in tow body

After the dry tests in lab and wet tests in acoustic test facility (ATF), a sea trial is carried out at Royapuram fishing harbor. A sample raw signal received in one channel during the sea trial is shown in Fig 11. In the figure, x- axis is number of samples and y- axis is the amplitude. Figure shows back scattered data acquired for 20 ms after a ping. Since the sampling frequency is 100 kHz, 20 ms data consists of 2000 samples. In the figure, multiple reflections are observable. The initial portion shows the direct reflection from the transmitter to the receiver. After a delay of approx. 800 samples, which correspond to 6 m depth, a number of reflections are observable. These correspond to the reflections from the sea bottom and successive buried sea bed layers and objects. A sample image generated by the sonar showing buried sea bed layers and protruded objects, during sea trials is shown in Fig 12.

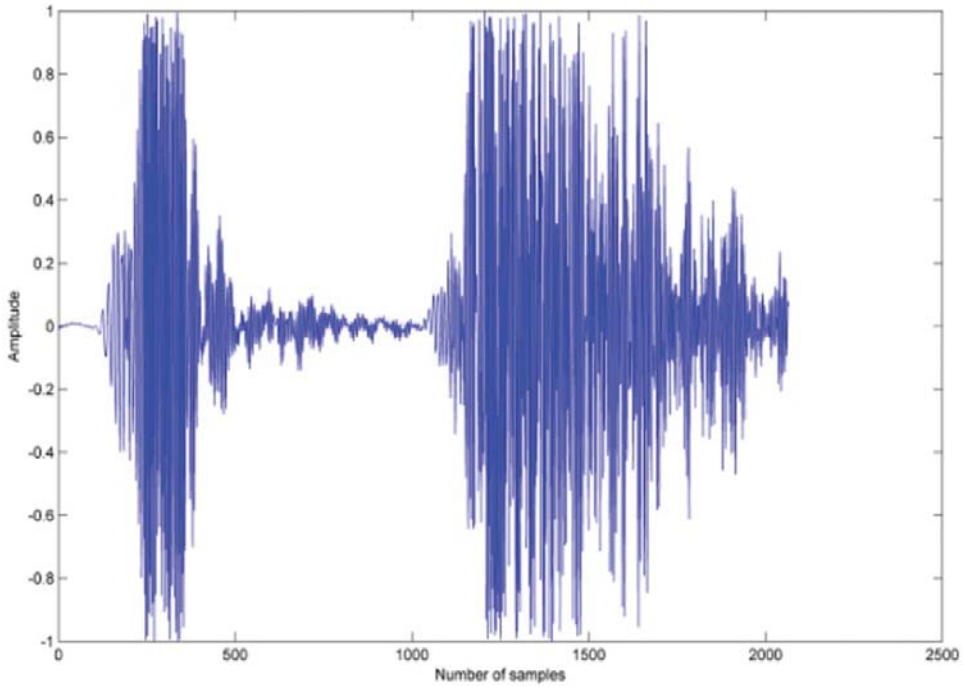

Fig. 11. Raw signal received in one channel

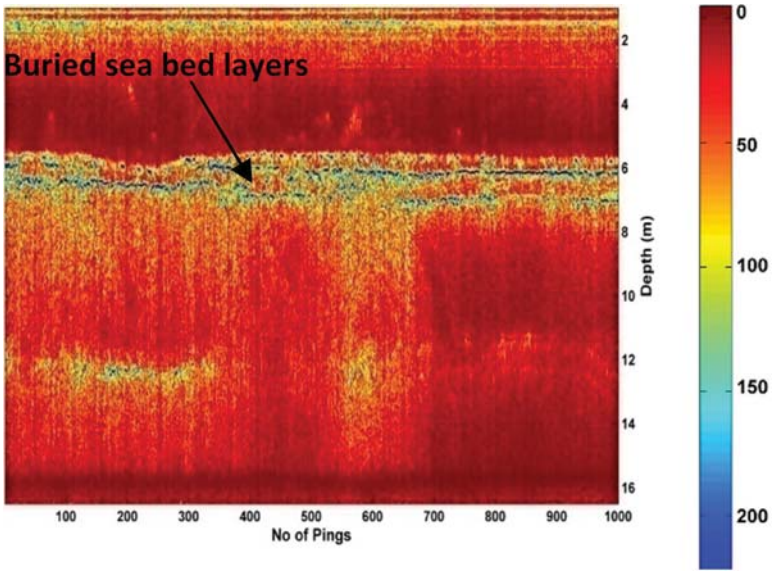

Fig. 12. Sub bottom profile generated with the sonar

5. CONCLUSION

FPGA based instrumentation scheme is devised for real time active buried object detection sonar. Indigenous design with common clock helps to maintain the critical time requirements for synchronizing various events in the sonar. Sonar signal generation and simultaneous acquisition of back scattered data from all the receiver hydrophone elements are synchronized with the common clock. Pings are geo referenced with position data from GPS. The system is designed to configure sonar operational parameters remotely through 10/100 Mbps Ethernet. After each ping, system acquires backscatter data and transfers in real time to the deck side signal processing unit through 10/100 Mbps Ethernet.

6. ACKNOWLEDGEMENTS

The authors would like to thank Mr. Prakash, Mr. Karthikeyan and Mr. Dileepan of the group for the system assembly and integration. Research and development on acoustic imaging systems is completely funded by the Ministry of Earth sciences, Govt. of India.

7. REFERENCES

[1] D.S. Sreedev, Dhilsha Rajapan, Shibu Jacob, Shijo Zacharia, P.M. Rajeshwari, K. Arumugam and M.A. Atmanand, 2018. "Design and Development of Real Time Wide Band Chirp Sonar for Detection of Buried Objects Under Sea Bed", *Proceedings of the International Conference on Sonar Systems and Sensors* (ICONS 2018), pp. 35-40.

[2] D.S. Sreedev, Dhilsha Rajapan, Shibu Jacob, Sayanti Bardhan, P.M. Rajeshwari, Shijo Zacharia and M.A. Atmanand, 2018. "Effectiveness of indigenously developed Chirp imaging SONAR in ship wreck detection", *MTS/IEEE Oceans* 2018, Kobe

[3] Sayanti Bardhan, Mahimol Eldhose, Dhilsha Rajapan, P.M. Rajeshwari, D.S. Sreedev, Shijo Zacharia, Kannan C., Shibu Jacob and M.A. Atmanand, 2015. "Detection of Buried Objects Using Active Sonar", *IEEE International Symposium on Underwater Technology -15*, Chennai, India

[4] S.G. Schock. "Buried Object Scanning Sonar," *IEEE J. Oceanic Eng.*, **26**(4).

[5] Martin Gutowski, Jerome Malgorn and Mark Vardy, 2015. "3D sub-bottom profiling - High resolution 3D imaging of shallow subsurface structures and buried objects", *Proceeding of Oceans 2015-Genova*

[6] Dhilsha Rajapan, 2013. "Acoustic imaging techniques and its applications", *Proceedings in the International Conference Acoustics* 2013, New Delhi

[7] R. Dhilsha, Sayanti Bardhan, D.S. Sreedev, S. Zakharia, M. Eldhose, S. Jacob and M.A. Atmanand, 2015. "Performance Comparison of Beamforming Algorithms for Buried Object Detection" *J. Acoustical Society of India*, **43**(1), 48-53.

[8] Mahimol Eldhose, Dhilsha Rajapan, Shijo Zacharia, D.S. Sreedev and M.A. Atmanand, 2015. "Techniques adopted in the post processing of active sonar data from Royapuram site-off Chennai", *Indian J. Geo-Marine Sciences*, **44**(2), 164-171

[9] S.G. Schock and J. Wulf, 2003. "Buried Object Scanning Sonar for AUVs", *Proceedings of Oceans 2003*, pp. 494-499.

[10] Godi Fischer, Alan J. Davis and Prasan Kasturi, 2007. "A Custom Chip Set for a Frequency-Agile High-Resolution Sonar Array", *IEEE J. Oceanic Engineering*, **32**(2).

[11] John E Ehrenberg and Thomas C Torkelson, 2000. "FM slide (chirp) signals: a technique for significantly improving the signal to noise performance in hydro acoustic assessment systems", *Elsevier Fisheries Research*, **47**, 193-199.

[12] Indian patent no. 288881, dt.30.10.2017 granted to National Institute of Ocean Technology

[13] C. Kannan, R. Dhilsha, P.M. Rajeshwari, Shibu Jacob and M.A.Atmanand, 2013. "Performance evaluation of cymbal hydrophones for underwater applications" *International J. Mechanical Engineering and Applications*, 1(2), 43-48.

The Journal of Acoustical Society of India : Vol. 45, No. 3, 2018 (pp. 121-130)

Signal processing aspects of an indigenous buried object detection sonar

Sayanti Bardhan, Mahimol Eldhose, Shibu Jacob, Shijo Zacharia, P.M. Rajeshwari and M.A. Atmanand

Marine Sensors Systems Group, National Institute of Ocean Technology
Pallikaranai, Chennai-600100, India
sayanti@niot.res.in

[Received: 20-09-2017; Revised: 15-04-2018; Accepted: 10-05-2018]

ABSTRACT

Indigenous development of Buried Object Detection SONAR (BODS), a system capable of detecting objects buried in the sea-bed, has been reported. To detect objects buried in sea-bed the BODS system utilizes a combination of low frequency and wide bandwidth and an array of customized signal processing algorithms. Signal processing algorithms like beamforming, matched filtering, hilbert transform forms vital steps to detection of objects buried in the seabed. This paper proposes the signal processing framework that aids in detection of the buried objects. Results from experiments at shallow water to detect buried targets like metal blocks, concrete plates and naturally buried stones are analyzed here. Detailed description of the BODS system algorithms with intermediate step-wise signal processing algorithm results are illustrated in this paper.

1. INTRODUCTION

Acoustic detection of underwater target is of great importance to civilian and naval applications. During the past few decade, attempts towards underwater imaging have been made by multibeam and sidescan sonars, but detection of buried objects still remain largely unexplored. The prime reason for this is volume scattering in suspended sediment layer and limited usefulness of high frequency in conventional sonar system[1-3]. Schock *et al.*[4] proposed detection of buried objects like cables, pipe section, ordnance and cylinders buried approximately at a depth of 0.3m in seabed on the east side of Oahu,with a bottom looking sonar of operating frequency of 5-23 kHz. Schock et.al.further reported[5] design and development of such sonars for Autonomous Underwater Vehicles. The system uses an array of 252 hydrophone elements and a 2-12 kHz transducer. However, till date no studies have been reported on indigenous design and development of sonar capable of buried object detection in the Indian subcontinent.

R. Dhilsha has reported[6] the advantages of lowering the frequency and larger bandwidth for real-time SONAR imaging systems using operating frequency of 2-24 kHz. Such an advantage has been further explored for indigenous development of a Buried Object Detection Sonar (BODS) system, for detection of buried objects in shallow water. BODS system detected objects like metal plate, concrete blocks, buried with human intervention, in the seabed of Royapuram Harbour, Chennai, Tamil Nadu[1].The work presented are the results of detection of buried objects by BODS system at Royapuram site with a water column depth of 5 m which is available at the site. The metal plate and concrete blocks buried at a depth of around 0.27 m

and 0.47 m respectively was reportedly detected by the system. The paper[1] also reports a signal penetration of 5 m in seabed of Cochin Port in Kerala, obtained by the BODS, where the water column depth is 11m. In continuation to detection of buried man-made objects, further results were reported[2], for detection of naturally buried rock structures by BODS system, in the Royapuram harbour located in the Bay of Bengal [Lat. 13.l3°N, Lon. 80.300E]. Also, reporting on detection of a partially buried ship wreck in shallow water by BODS system is made[3].

For BODS system, processing of the signal acquired by the receiver hydrophones forms a vital subsystem that enables it to detect and image objects that are buried in seabed[7-9]. Time-space approach like beamforming and their applications in array signal processing has been reported earlier[10-12]. However adoption of such processing for sonar systems and customization of the algorithms to suit the need of BODS is a crucial step in the design of the BODS system. BODS signal processing involve beamforming, matched filtering and Hilbert transform as the three vital signal processing steps. This paper reports the details and the flowchart of the signal processing algorithms of the BODS system.

2. SYSTEM DESIGN

The BODS system operates in a wideband frequency range of 2-24 kHz. The transmitting signal is a Frequency Modulated pulse with a pulse length of 3 m sec. The BODS system can be further sub-divided into two prime subsystems: Tow Body and Deck system. The tow body contains an acoustic transmitter, four receiver hydrophone arrays, a signal generator, motion sensor, GPS receiver, power supplies and power amplifier for data collection and streaming. The deck side of BODS contains data processor for signal processing and image generation.

The 1.75 m × 0.70 m × 0.30 m stable floating tow body houses the transducer[13] and receiver hydrophone arrays[14-17]. The electronic subsystems in the tow body are contained in two water proofed enclosures. Each hydrophone input has a dedicated pre-amplifier, anti-aliasing low pass filter, a programmable gain amplifier (PGA), an Analog-to-Digital Converter (ADC), where each ADC samples the data at 100 kHz with a resolution of 16 bits.

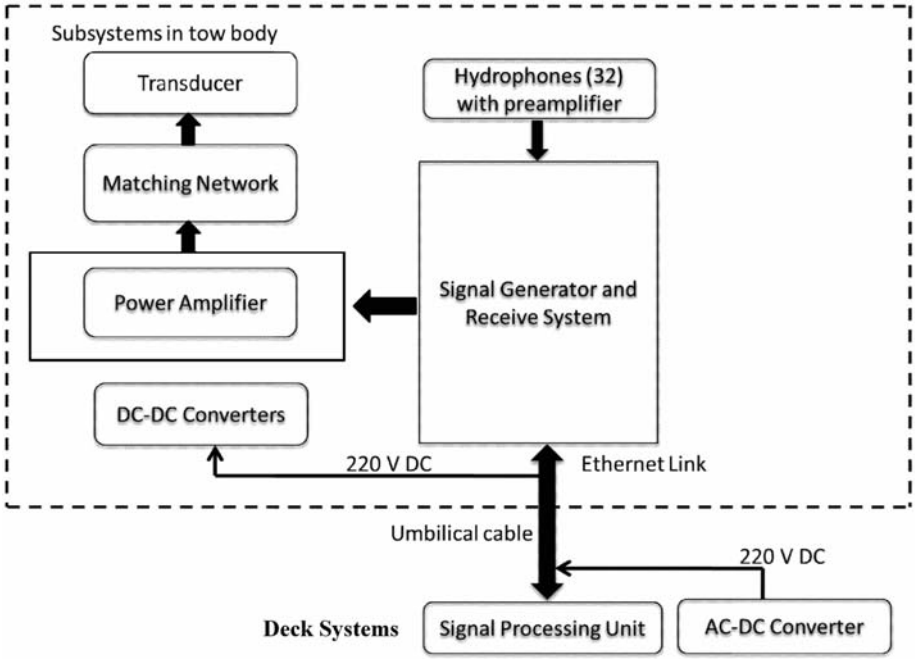

Fig. 1. Block diagram of the BODS system

The link between the two subsystems, the tow body and the deck side is established by the umbilical tow cable having conductors for power and ethernet. Converted data over an ethernet interface is sent to deck data processor for processing and image generation. The general block diagram of the BODS system is given in Fig 1. In the deck side of BODS, signal undergoes an array of signal processing algorithms that converts the raw acoustic signal to an image where the buried object can be located. A further detail of the signal processing algorithms is given in Section 3.

3. SIGNAL PROCESSING

3.1 Data format

The deck side of the BODS system stores the received raw acoustic data and processes it for real-time image generation. For processing of the signals, imaging, storage and display of the final image we use an industrial laptop with Core i7 - 2600 3.4GHz processor with 8 cores and 500GB hard disc. Binary files are received by the signal processing unit at the deck side of the BODS system and are processed to obtain channel wise data for further ease of data processing, *i.e.,* for 16 channel hydrophone data, the binary files are converted to a 16 column data.

Further the raw data from each channel corresponds to 3456 samples and is stored in a matrix format. The raw data is rearranged as matrix of [3456 × 16] where 16 correspond to total number of channels with 3456 samples per channel and 55296 is total number of samples per ping of data. The raw data is saved for consecutively 1000 pings. Finally, the raw data for processing is in the form 55296 × 1000. This raw data is fed to the array of signal processing algorithms.

3.2 Signal Processing Algorithms

A block diagram showing the signal processing algorithms of the BODS system that enables it in imaging buried objects is given in Fig 2. The vital algorithms include Delay and Sum Beamforming[18-19], Match Filtering[20] and Hilbert Transform[21-22], as given below.

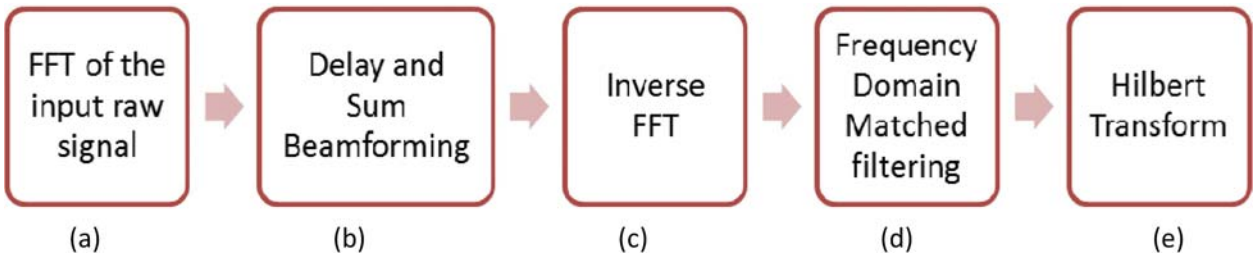

Fig. 2. Block Diagram of signal processing algorithms of BODS

The signal processing algorithms are implemented in MATLAB in the deck end industrial laptop. In real time, a binary file gets created by the data acquisition receiver subsystem. As soon as a binary file is created, MATLAB reads the binary file and separates the channel wise data corresponds to each ping.

The beamformer currently used in the BODS system is Delay and Sum Beamformer. Delay and Sum Beamformer uses delays between each array element that compensate for differences in propagation delay of the desired signal across the array. Signals originating from a desired direction are summed in phase, while other signals undergo destructive interference[18]. The delay and sum beamformer output[19] is given by

$$y(k) = \sum_{L=1}^{J} \sum_{p=0}^{K-1} w_{L,p}^{*} x_L(k-p) \quad (1)$$

Where y(k) is the output at any time k, K-1 is the number of delays for J sensor channels and w* represents

the conjugate of the weights applied to each element. The normalized wide band signal data undergoes a band-pass filtering of 2-24 kHz. The filtered signal is transformed at each sensor into frequency domain by Fourier Transform of the signal, as given in Fig. 2a. After beamforming of the signal in Fig. 2b at each frequency bin, inverse Fourier Transform produces the output time series, as shown in Fig. 2c.

The output of the beamforming algorithm is fed to the match filter. The match filter helps in improving the signal-to-noise ratio (SNR) of the signal by matching the signal received to the template of the chirp signal in Fig 2d. For BODS system, a frequency domain match filter is programmed and implemented. Here, the match filter output is obtained as a product of complex conjugate of the transmitted signal and FFT transformed received signal[20]. For further processing the final output of the match filter is transformed back to time domain.

The time domain match filtered output is fed to the Hilbert transform, as given in Fig 2e. Hilbert transform facilitates computation of the pulse envelope of the match filtered output. Hilbert transform is a linear operator[21-22] that aids in final visualization of the distinct echo contributions in the time domain. Hilbert transform output is guided by the following equations:

$$H(f_n) = \hat{f}_k = \begin{matrix} \frac{2}{\pi}\sum_{n\ odd}\frac{f_n}{k-n},\ k\ even \\ \frac{2}{\pi}\sum_{n\ even}\frac{f_n}{k-n},\ k\ odd \end{matrix} \quad (2)$$

where, f_n is the output from match filter and n represents the number of samples. The Hilbert transformed output is finally mapped ping by ping to custom made image matrix, which form the final output of the BODS system. In the final BODS imaging a two stage imaging is done. First the BODS system software generates a 256 scale colour map that assigns colours according to the signal intensity. Then the entire 256 colour scale is transformed to 8 colour scale such that a band of signal intensity is demarcated by a single colour. This 8 colour scale signal intensity is converted to dB scale. The dB scale forms a part of the final BODS image. Each acoustic signal return corresponds to a certain dB value that is further demarcated by the colour scale given. Further processing of the signal in dB scale is in progress and will be presented in subsequent publications.

4. EXPERIMENTAL DETAILS

Results analysed in this paper are from sea trials conducted in the Royapuram Harbour, Off Chennai in Tamil Nadu, India [Lat. 13.07°N, Lon. 80.18°E] on 24-28 June, 2014 with the BODS system. Sediment type at the site was clay mixed with sand and water column depth available at the site varied from 5 m to 10 m. Two experiments were conducted with buried objects. Objects like metal (mild steel) plate and concrete blocks were buried with human intervention in the seabed of Royapuram site location. Simultaneously attempts were made to detect naturally buried rock structures, buried in Royapuram seabed. The term 'naturally buried' here refers to the stone structures fallen from seashore and buried in the due course of time in Royapuram Harbour seabed.

Both metal plate and concrete blocks are buried side by side for the feasibility of towing. The dimensions of the objects buried are given in Table 1. Twenty concrete blocks arranged in five rows and two columns and is buried about 0.47 m in the seabed. Each block has a dimension of 0.3 m × 0.3 m × 0.02 m, and hence the entire concrete block set is of the dimension 1.5 m × 1.2 m × 0.02 m.

Table 1. Dimensions of the objects buried

Sl. no.	Type/ Name of the object	Dimension
1	Metal plate	1 m × 1 m × 0.01 m
2	Concrete blocks	1.5 m × 1.2 m × 0.02 m

5. RESULTS AND DISCUSSIONS

BODS Imaging: Fig. 3 shows the image from the Royapuram Harbour with the buried metal plate and the concrete blocks. The water column depth as seen in Fig. 3 is around 5 m. These objects were buried by human intervention with the help of scuba divers during the experiments. On the other hand, Fig. 4 shows the image from Royapuram Harbour with naturally buried stone structures. The water column depth as observed there is around 6 m. Fig. 4 is an experiment conducted with naturally buried object, in contrast to Fig. 3 that is an experiment conducted with objects buried with human intervention.

In both Fig. 3 and 4 the received signal undergoes Beam forming, Match Filtering and Hilbert Transform, as described in section 3, to give the final image. The x-axis in both the figures indicates ping no. and the y-axis indicates the depth. In both Fig. 3 and 4 images are generated for upto 1000 pings. In Fig. 3, the metal

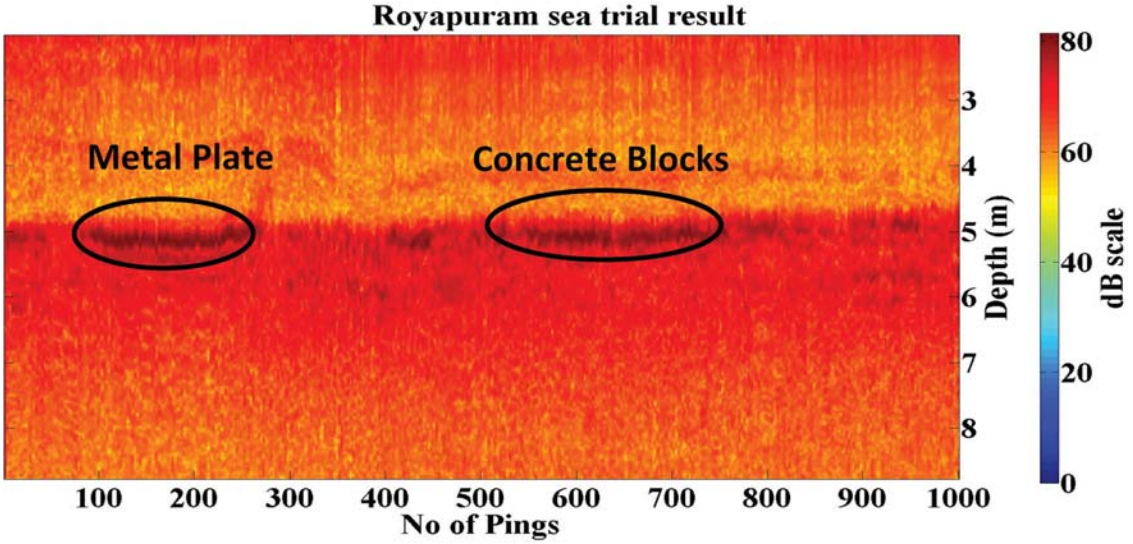

Fig. 3. Metal plate and concrete blocks detected by BODS

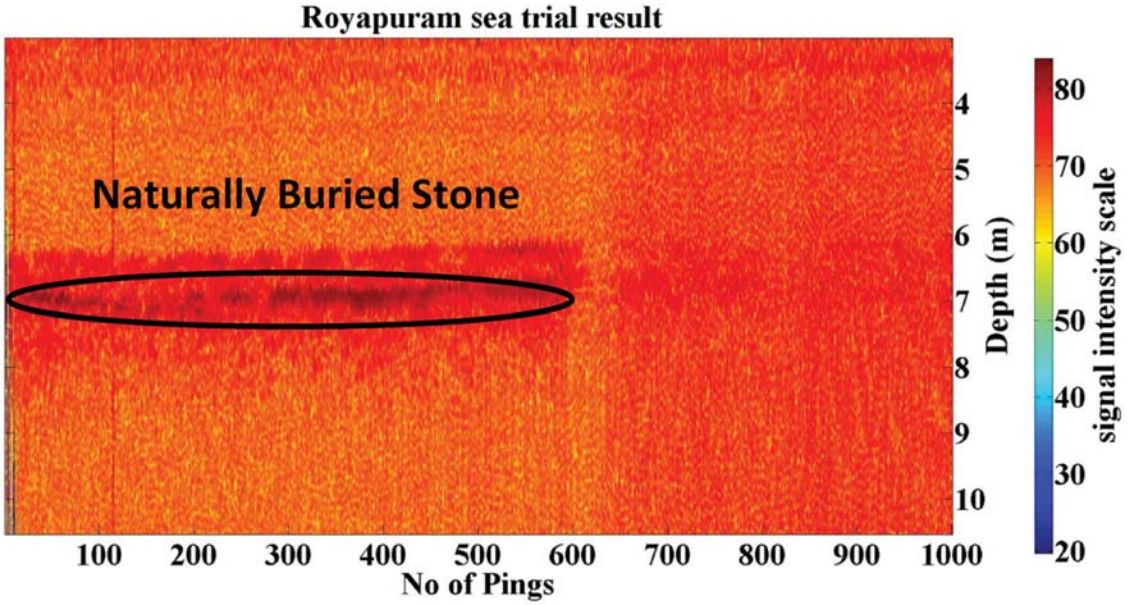

Fig. 4. Naturally buried stones detected by BODS

plate is detected between ping no. 108 to 224 and the concrete blocks are detected between the ping no. 573 to 715. The detected metal plate and concrete blocks have been encircled in Fig. 3. In Fig. 4, naturally buried objects are detected between ping no. 1 to 600 and the detected naturally buried stones are encircled too in Fig. 4.

Signal level output : Analysis of the signal received for metal & concrete plate detection and naturally buried stone detection is further conducted and presented in this paper. For the metal and concrete dataset, one ping representing the reflection from metal plate and one ping from the concrete blocks reflection is shown below. Fig. 5 gives the beamformed output for ping no. 167 that corresponds to the metal plate and Fig. 6 gives the beamformed output for ping no. 602 that corresponds to the concrete plate. The x-axis gives the number of samples and the y-axis gives the signal intensity here. In fig. 5, the first signal between sample no. 330-825 corresponds to energy generated by the air-water interface and the sample no corresponding to 1075-1456 refers to the signals reflected from the buried metal plate. In fig. 6, the sample no. 384-812 corresponds to the air water interface and the sample no. within 1060-1592 corresponds to the concrete blocks.

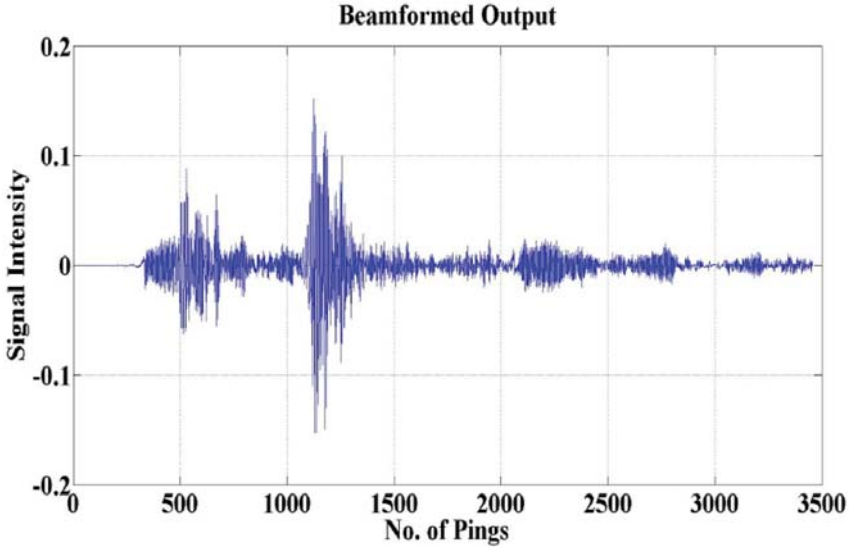

Fig. 5. Beamformed output for ping no.167 (metal plate)

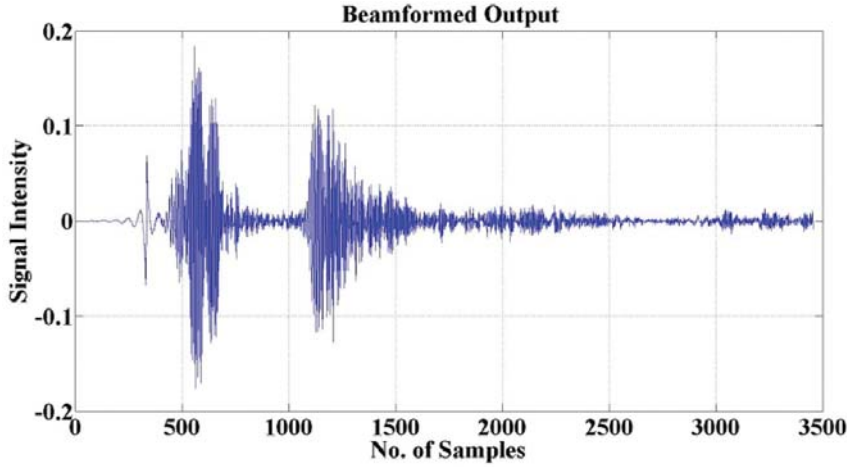

Fig. 6. Beamformed output for ping no.602 (concrete blocks)

Fig. 7 gives the matched filtered output of the ping no. 167 (metal plate) and Fig. 8 gives the matched filtered output for the ping no. 602 (concrete blocks). The x-axis here also gives the no of samples and the y-axis gives the signal intensity. The first reflection between the sample no. 330-825 in Fig. 7 refers to the first reflection received by the BODS system due to the air-water interface. The second reflection between the sample no. 1075-1456 refers to the reflections from the detected buried objects. It can be seen that in comparison to the beamformed output, the matched filtered output amplifies these first two reflections and supresses the reflections after ping no. 1500, which doesn't lie in the detection objective of the BODS system, and is hence noise for the system. Thus it can be seen that matched filtering certainly increases the signal to noise ratio.

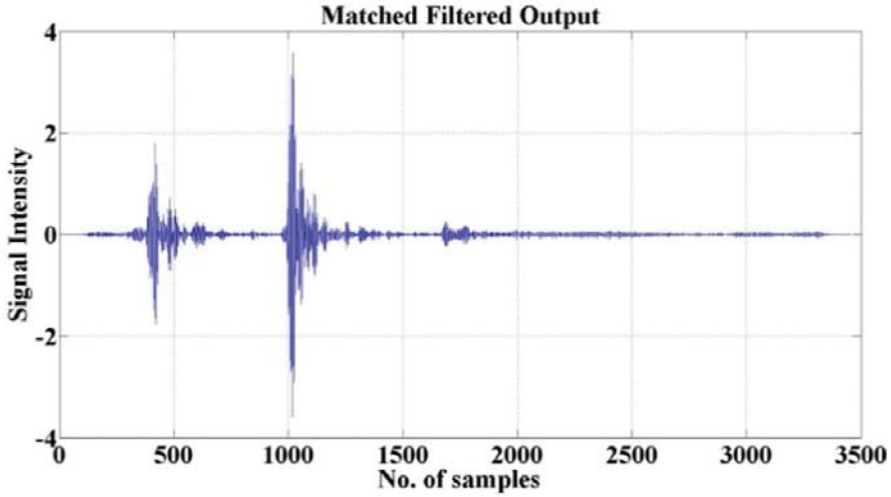

Fig. 7. Matched Filtered output for ping no. 167 (metal plate)

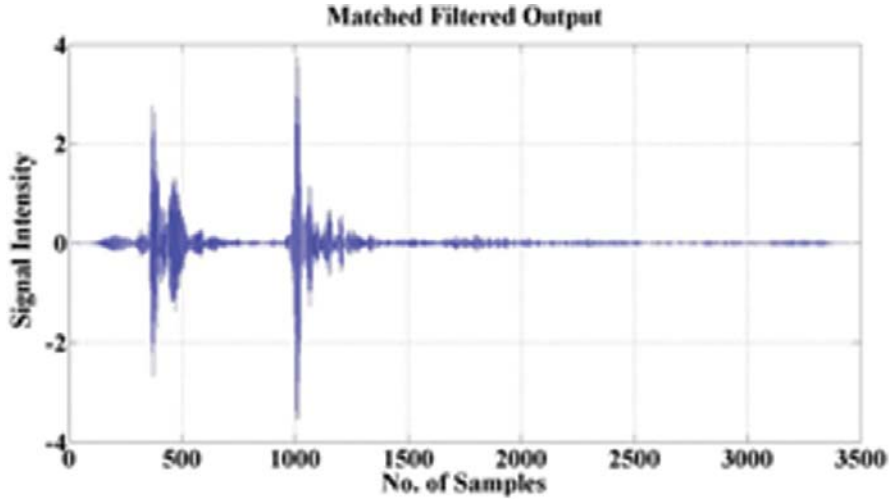

Fig. 8. Matched Filtered output for ping no. 602 (concrete blocks)

Fig. 9 and 10 gives the analysis of the naturally buried stone dataset. The beamformed output of the naturally buried stone is given in Fig. 9 for ping no. 400 and the matched filtered output for the same ping is given in Fig. 9. The signal corresponding to sample no. 993-1500 corresponds to the naturally buried stone and hence 400-th ping is randomly chosen to represent the naturally buried stone. The matched

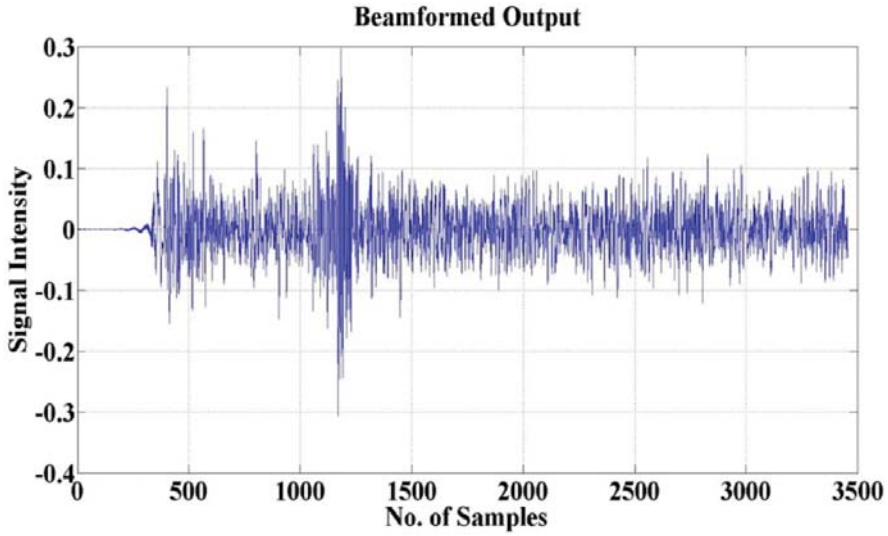

Fig. 9. Beamformed output of ping no. 400

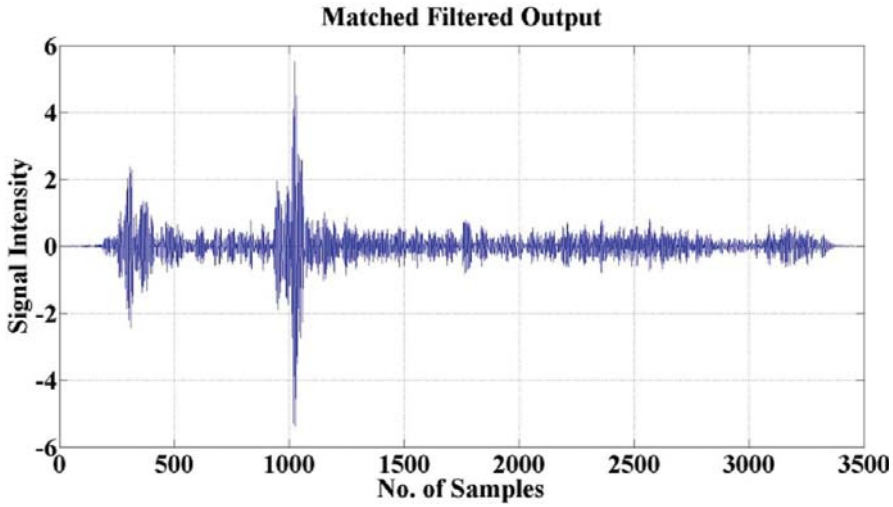

Fig. 10. Matched Filtered output of ping no. 400

filtered signal, given in Fig. 7, 8 and 10, undergoes hilbert transform to give the final image shown in Fig. 3 and 4. Each ping undergoes each of the above mentioned steps of processing to give the final output. The time required by the proposed sonar signal processing algorithm to process 1000 ping data is 172.41 sec.

The figures given above shows graphical representation of signals of the intermediate output for the signal processing steps like beam forming, matched filtering. The signal transformation that leads to detection and imaging of buried objects is evident.

6. CONCLUSION

The results show BODS system detecting the metal plate, concrete blocks and naturally buried stones. The paper proposes signal processing algorithms required for the detection of such buried objects. The signal

processing framework is detailed in the paper and a flowchart providing the sequence of the algorithm is described in the paper. The paper reports intermediate results of the signal processing algorithm like beamforming and the matched filtered output. This provides an insight into the signal level transformation that finally gives the image with the buried objects.

7. ACKNOWLEDGEMENTS

The authors would like to thank team members of the Marine Sensors and System Group who helped in carrying out the field trials successfully. This work is funded completely by National Institute of Ocean Technology (NIOT), Ministry of Earth Sciences, Govt. of India.

8. REFERENCES

[1] S. Bardhan, Dhilsha Rajapan, Shijo Zacharia, Mahimol Eldhose, P.M. Rajeshwari, D.S. Sreedev, C. Kannan, Shibu Jacob and M.A. Atmanand, 2015. Detection of buried objects using active sonar, *International Symposium on Underwater Technology, Chennai, India*.

[2] Sayanti Bardhan, R. Dhilsha, Shibu Jacob, D.S. Sreedev, Shijo Zacharia, P.M. Rajeshwari, K. Arumugam and M.A. Atmanand, 2018. Detection of underwater rock structures by Indigenously developed SONAR system, *International Conference on Sonar systems and sensors, Kochi*.

[3] D.S. Sreedev, Dhilsha Rajapan, Shibu Jacob, Sayanti Bardhan, P.M. Rajeshwari, Shijo Zacharia and M.A. Atmanand, 2018. Effectiveness of indigenously developed Chirp imaging SONAR in ship wreck detection, *IEEE OCEANS, Kobe, Japan*.

[4] Steven G. Schock, Arnaud Tellier, Jim Wulf, Jason Sara and Mark Ericksen, 2001. Buried Object Scanning SONAR, *IEEE Journal of Oceanic Engineering*, **26**(4), 677-689.

[5] S. Schock and J. Wulf, 2003. Buried Object Scanning SONAR for AUV's, *IEEE OCEANS, San Diego, USA*.

[6] Dhilsha Rajapan, 2013. Acoustical Imaging Techniques and its Applications, Acoustics, New Delhi.

[7] R. Dhilsha, Sayanti Bardhan, D.S. Sreedev, S. Zakharia, M. Eldhose, S. Jacob and M.A. Atmanand, 2015. Performance of Beamforming Algorithms to detect Buried Objects in seabed, *National Symposium on Acoustics, Goa*.

[8] Sayanti Bardhan and S. Jacob, 2015. Experimental Observations of Direction of Arrival Estimation Algorithms in a Tank environment for Sonar Applications, *IEEE International Symposium on Ocean Electronics,* Cochin University of Science & Technology, Kochi.

[9] Dhilsha R., Sayanti Bardhan, D.S. Sreedev, S. Zakharia, M. Eldhose, S. Jacob and M.A. Atmanand, 2016. Performance Comparison of Beamforming Algorithms for Buried Object Detection, *Journal of Acoustical Society of India,* **43**(1), 48-53.

[10] B.D. Van Veen and K.M. Buckley, 1988. Beamforming: A versatile approach to spatial filtering, *IEEE ASSP Magazine,* **5**(2), 4-24.

[11] J.E. Piper, 2011. Sonar Systems, In Tech Publishing.

[12] H. Krim and M. Viberg, 1996. Two decades of array signal processing research: the parametric approach, *IEEE Signal Processing Magazine*, **4**(13), 67-94.

[13] Dhilsha Rajapan, 2002. Performance of a low-frequency, multi-resonant broadband Tonpilz transducer, *J. Acoust. Scoc. Am.*, **111**(4), 1692-1694.

[14] C. Kannan, P.M. Rajeshwari, Shibu Jacob, A. Malarkkodi, R. Dhilsha and M.A. Atmanand, 2011. Effect of manufacturing procedure on the miniaturized Flextensional Transducers (Cymbals) and hydrophone array performance, *IEEE OCEANS, Spain*.

[15] R. Dhilsha, P.M. Rajeshwari and M. Sankar, 2009. Underwater performance of a 5 × 10 cymbal array for oceanographic applications, *ICOE Proceedings, Chennai*.

[16] Dhilsha Rajapan, P.M. Rajeshwari, M. Sankar, K. Trinath and N.S. Prasad, 2006. Miniaturized underwater sensors for the realization of Conformal arrays, *IEEE OCEANS, Singapore*.

[17] C. Kannan, R. Dhilsha, P.M. Rajeshwari, Shibu Jacob and M.A. Atmanand, 2013. Performance Evaluation of Cymbal Hydrophones for Underwater Applications, *International Journal of Mechanical Engineering and Applications,* **1**(2), 43-48.

[18] J. Benesty, M.M. Sondhi and Y. Huang, 2008. Springer Handbook of Speech Processing, *Springer*.

[19] Barry D. Van Veen and Kevin Buckley, 1988. Beamforming: A Versatile Approach to Spatial Filtering, *IEEE ASSP Magazine,* **5**(2), 4-24.

[20] George L., 1960. An introduction to matched filters, *IRE Transactions on Information Theory*, **3**(6), 311-329.

[21] S.L. Marple, 1999. Computing the Discrete-Time Analytic Signal via FFT, *IEEE Transactions on Signal Processing,* **47**(9), 2600-2603.

[22] V. Cizek, 1970. Discrete Hilbert Transform, *IEEE Transactions on Audio and Electroacoustics*, **4**(58), 585-586.

The Journal of Acoustical Society of India : Vol. 45, No. 3, 2018 (pp. 131-140)

Target detection of buried object scanning SONAR images using Artificial Bee Colony based Tsallis entropy

P.M. Rajeshwari, Dhilsha Rajapan, Mahimol Eldhose and A. Karthikeyan
Marine Sensors Systems Group, National Institute of Ocean Technology
Pallikaranai, Chennai-600100, India
pmr@niot.res.in

[Received: 20-09-2017; Revised: 15-04-2018; Accepted: 10-05-2018]

ABSTRACT

Autonomous underwater vehicles are integrated with SONAR for applications such as obstacle avoidance, detection of lost objects buried / lying on the seabed, and profiling of seabed in deep waters where a diver cannot be employed to execute. An automatic target detection algorithm is required to detect the targets. In volumes of data, detecting the target manually is cumbersome and a monotonous exercise. In the present work, detection is carried out using Artificial Bee Colony (ABC) based Tsallis entropy method, with and without preprocessing method for Buried Object Scanning SONAR image (BOSS). This method is implemented for BOSS images for the first time and reported. Entropic index is varied from 0.1 to 2 for Tsallis algorithm. Optimum performance is obtained at a value of 0.1. Maximum objective function value of 6506 is observed for segmentation with preprocessing method. The corresponding threshold is 127. Marginal difference in objective function values of 6 to a maximum of 150 is observed for the considered images with and without preprocessing. The algorithm was carried on the dataset acquired from the indigenously developed BOSS system of NIOT, India. The object considered for the detection is the mild steel plate of dimension (1m × 1m × .01m).

1. INTRODUCTION

SONAR (Sound Navigation and Ranging) transmit sound waves and from the reflected echo signals, detection is carried out. SONAR is employed for bathymetry applications, fish finding, sub bottom profiling, imaging sea floor variations[1], obstacle avoidance in forward looking SONARs, integrated with autonomous underwater vehicle (AUV) to investigate seabed characteristics, underwater structures[2,3]. Automatic target detection is essential for defense applications and to assist human operator in classification of targets [4,5].

Segmentation is carried out prior to classify the objects of interest[6]. Xiu Fen *et al.*[7] proposed segmentation using Gaussian Markov random field based texture feature extraction integrated with level set. A modified level set using top and bottom hat transform as preprocessing and level set segmentation is reported by Guangyu *et al.*[8]. Turgay Celik *et al.*[9] proposed preprocessing using un decimated wavelet transform and segmentation using k means algorithm for the feature extracted from wavelet transform. Particle swarm optimization with Fuzzy c- Means clustering segmentation is carried out by Liu Hongpo *et al.*[10] for SONAR

images. Bilevel and multilevel threshold Otsu based segmentation for gray image using Bats algorithm is suggested by V. Rajinikanth *et al.*[11].Fuzzy approach with Tsallis entropy for gray and color image is implemented by Samy Sadek *et al.*[12]. Multilevel threshold for camera images was applied by Manikantan *et al.*[13] using modified Particle swarm optimization (PSO) method and Genetic algorithm. Both methods were compared for its performance. Batool Pouryani *et al.*[14] recommended preprocessing using Contourlet transform for side scan SONAR images. Features was extracted and using data mining, Cummins clustering classification method segments the image. Min cut maximum flow graph cut segmentation is carried on the segmented image output of Iterative Conditional Mode method by Raquel *et al.*[15]. Bahriye Akai[16] followed segmentation using PSO and ABC optimization methods. Kapur's entropy and Otsu method were used as fitness functions to detect optimum threshold for standard test images. Local binary fitting active contour for SONAR images is proposed by Enfang Sang *et al.*[17] to detect weak edges of object and shadows efficiently. But this method is sensitive to the initial condition which should be set closer to the target[18].

Various types of entropy method and its applications are described by Nitin Chamoli *et al.*[18]. It is suggested that, Tsallis entropy method suits best for gray level distribution with unimodal histogram[19]. Firefly algorithm based Tsallis and Kapur entropy method is studied by Suresh Manic *et al.* 1920. The study implies that Tsallis method performed better when compared to Kapur method. Vaishali R. Kulkarni *et al.*[21] has reported that ABC based optimization method produces more accurate results when compared to Particle swarm optimization. To summarize about image segmentation methods, there is no single method which can suit all types of images[22].

The motivation in the present work is to study the performance of segmentation with and without preprocessing with ABC based optimization method. This is a preliminary work carried out to detect the targets. Classification of targets will be carried out in near future since volumes of data are required to create a database. To classify, robust feature extraction becomes essential. As an initial work, bilevel threshold is implemented to extract the objects buried in the sediments of the sea bed and from the water column. The paper is organized as follows. Section 2 focuses on methodology of image acquisition, Tsallis entropy, and ABC algorithm. Section 3 portrays about the results and discussion. Finally section 4 concludes the paper.

2. SYSTEM DESIGN

2.1 Methodology of Image acquisition

BOSS is employed to detect the buried objects in the sea floor. The BOSS principle is to transmit pulsed chirp signals in the frequency range 2kHz-16kHz. This wide band signals drives the transducer with high power using power amplifier. Piezo electric transducers convert electrical power into sound waves to dissipate into the ocean. The received pressure waves are converted into electrical signals using hydrophone array. This pulse gets reflected from the ensonified area of the seabed and from the objects buried. The received pressure signals are converted with the hydrophone array. Multi input data acquisition acquires the back scattered signals. Appropriate signal processing methods are used to generate the image. Every transmission and reception of signals is called pings. Collection of pings are framed together to form an image[23]. For detection of the buried object, the objects / targets should be highly reflective in nature and the impedance match between the sediment and the object should be more to be detected.

The database images are from the indigenized Buried object scanning SONAR system developed by NIOT. Mild steel plate of size 1 m × 1 m × .01 m is buried. Fig 1 displays the mild steel plate before burial. The survey was conducted at Royapuram off coast Chennai. Fig 2 portrays the tow fish incorporated with transducers The tow fish integrated with transmitter and hydrophones was towed behind the vessel at a speed of 2 knots Fig 2 portrays the tow fish incorporated with transducers.

2.2 Pre-processing

Prior to segmentation, pre-processing is required to filter noise [24] or contrast enhancement is required

Fig. 1. Snap shot of mild steel plate before burial

Fig. 2. Tow fish integrated with Transmitter and hydrophones

[25]. In the present work, unsharp filter with alpha value 0.2 is used to enhance edges. The unsharp mask [26] in MATLAB is given by

$$\frac{1}{(\alpha+1)}\begin{bmatrix} -\alpha & \alpha-1 & -\alpha \\ \alpha-1 & \alpha+5 & \alpha-1 \\ -\alpha & \alpha-1 & -\alpha \end{bmatrix} \tag{1}$$

Using this kernel, image is correlated with the MATLAB function 'imfilter'. The resultant image generated is the edge sharpened image with contrast enhancement.

2.3 Tsallis Entropy algorithm

Tsallis entropy [27] maximizes the information between the two categories (object and background pixels) and is defined as

$$T_{opt} = \arg\max[S_q^A(t) + S_q^B(t) + (1-q)S_q^A(t)S_q^B(t)] \tag{2}$$

where $s_q^A(t) = \frac{1-\sum_{i=0}^{t-1}\left[\frac{P_i}{P^A}\right]^q}{q-1}$; $s_q^B(t) = \frac{1-\sum_{i=t}^{255}\left[\frac{P_i}{P^B}\right]^q}{q-1}$; *'q'* is the entropic index[28] which is the measure of degree of non-extensivity of the system. Pi is defined as the probability density function for the given image with L (255) levels and is given by

$$P_i = \frac{h(i)}{N},\ (0 \le i \le L-1) \tag{3}$$

where N are the total number of pixels in the considered image. Entropic index[28] 'q' is varied from q<1 to q >1.

2.4 Artificial Bee Colony Algorithm

Evolutionary algorithms are used to determine optimum solution in less time[29]. ABC [30,31] is one of the meta heuristic algorithm applied to determine threshold values by maximising the objective function of Tsallis entropy method. Three type of bees are employed namely employee, onlooker and scout bees.

In the present work, 20 onlooker bees and 20 employee bee are employed for detection of threshold to delineate the object pixels from the background. The algorithm steps are as follows:

1. The number of population 'n' is selected
2. Threshold values are generated randomly for 'n' population and is given by

$$x_{ij} = x_{\min,j} + rand\,(0,1)\,(x_{\max,j} - x_{\min,j}) \tag{4}$$

   where i = 1, 2, ...n; n = number of threshold values for employees bees and j = dimension to be determined by the optimization algorithm.

3. For the generated random values, fitness values is evaluated using equation 1
4. The thresholds are updated by performing a local search and is given by

$$v_{ij} = x_{ij} + \phi_{ij}(x_{ij} - x_{kj}) \tag{5}$$

   where i = 1, 2…n; n = population of bees; $ø_{ij}$ = rand (-1, 1); j = dimension and k = rand (1, n)

5. Greedy selection is performed between the initial fitness evaluated and the fitness generated by local search
6. The probability calculation is evaluated and is given by

$$P\{x_i\} = \frac{f(x_i)}{\sum_{i=1}^{n} f(x_i)} \tag{6}$$

   where $f(x_i)$ is the fitness values obtained

7. Solution is selected based on the probability of the onlooker bee.
8. On looker bees are employed for exploring better solution and is given by

$$v_{ij} = x_{ij} + \phi_{ij}(x_{ij} - x_{kj}) \tag{7}$$

   where i =1, 2…n; n is the number of population; $ø_{ij}$ is generated from rand (-1, 1); j is the dimension and k is the random generated

9. Fitness is again evaluated for greedy selection between solution based on probability and from onlooker bee solution
10. Scout bees keep monitoring for any stagnation of same solution.
11. If solution stagnates, new solution is generated and is given by

$$x_{ij} = \min(x_{ij}) + rand\,(0,\ 1)\,(\max(x_{ij}) - \min(x_{ij})),\ counter \ge \lim it = x_{ij},\ else \tag{8}$$

where min(x_{ij}) is the lower limit and max(x_{ij}) is the upper limit of thresholds and limit is the number of times, thresholds can stagnate

12. Steps 3 to 11 are carried out till convergence is attained.

3. RESULTS AND DISCUSSIONS

Fig. 3 shows the image from the Royapuram Harbour with the buried metal plate A typical Buried object scanning SONAR image considered for target detection is shown in Fig 3 (Image 1). The image depicts a mild steel plate buried in sediment at a depth of 15 to 25 cm beneath the seabed. All the considered images were subjected to contrast enhancement. The enhanced image serves as an input to ABC algorithm for determination of threshold. BOSS generates vertical cross section of the sea bed. Sea floor is detected at a depth of approximately 4 m. The image represents the buried object mild steel plate. Dark pixels between pings 270 to pings 300 portrays the object, mild steel plate buried at a depth of 4.5 m from the water column. Some debris are naturally buried in the seabed observed at a depth of 5 m. Unearthing is really a task in the field.

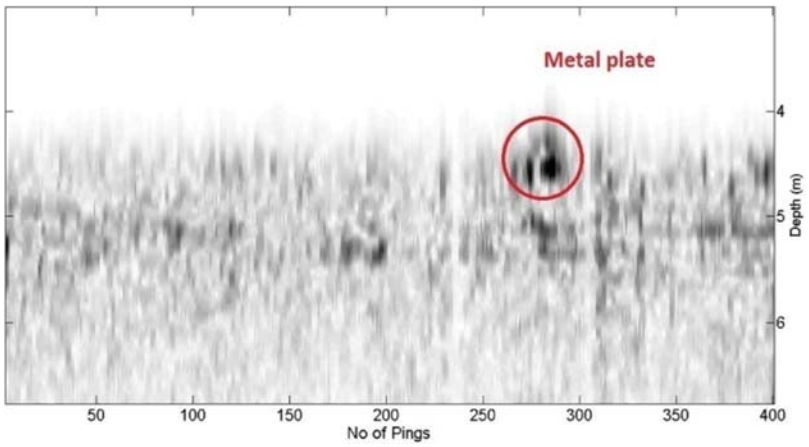

Fig. 3. Image of the mild steel plate buried

The histogram for the considered image is displayed in Fig 4. After sharpening the image, the modified histogram is depicted in figure 5. From Fig 5, it is observed that after contrast enhancement, histogram probability density function has reduced ripples in the intensity range of 200 to 255.

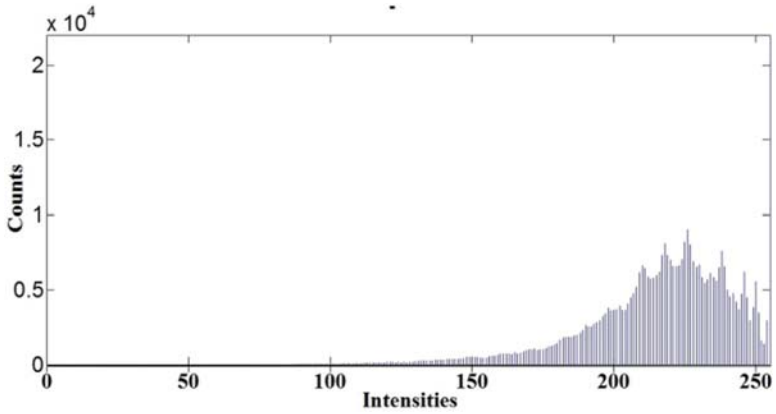

Fig. 4. Histogram output of the mild steel plate

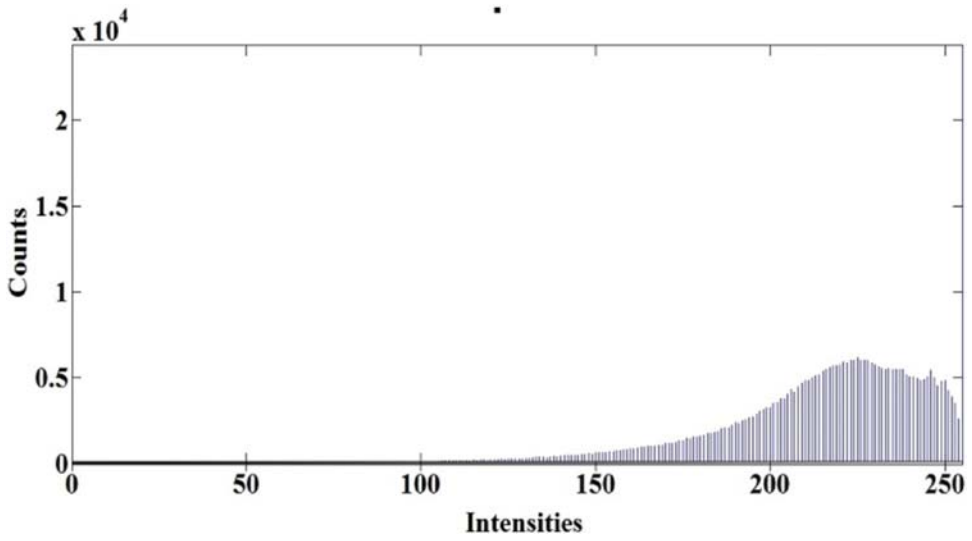

Fig. 5. Histogram the enhanced image of mild steel plate

Fig. 6 shows the segmented output of the buried object of mild steel plate for 'q' value of 0.1. It is observed that, the algorithm is able to detect the object alone from the sediments and the water column. The threshold value is determined as 127 from ABC based Tsallis algorithm.

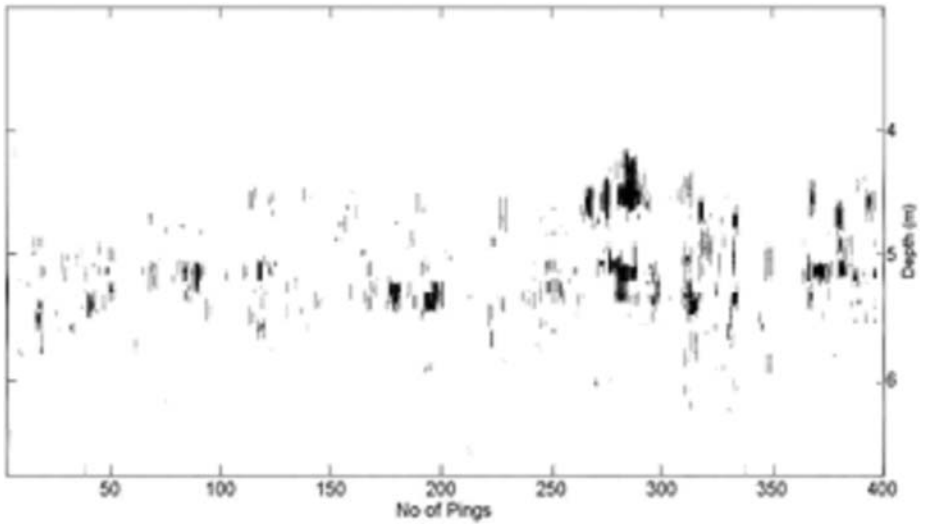

Fig. 6. Segmented output (q = 0.1) of buried object (mild steel plate)

Fig. 7 shows the trajectories of the bee population towards convergence to determine thresholds. In the present work, 30 iterations was carried out for convergence. It is observed that at 15th iteration, convergence is observed. Moreover objective function remains constant after 15th iteration signifying convergence. A maximum objective function value of 6319 is observed for a threshold of 127.

Fig. 8 shows the objective function value variation for the images carried out for with and without pre-processing for an entropic index value of 0.1. An enhanced value of objective function indicates that with pre-processing, detection of targets is enhanced as the Tsallis algorithm states maximum objective function

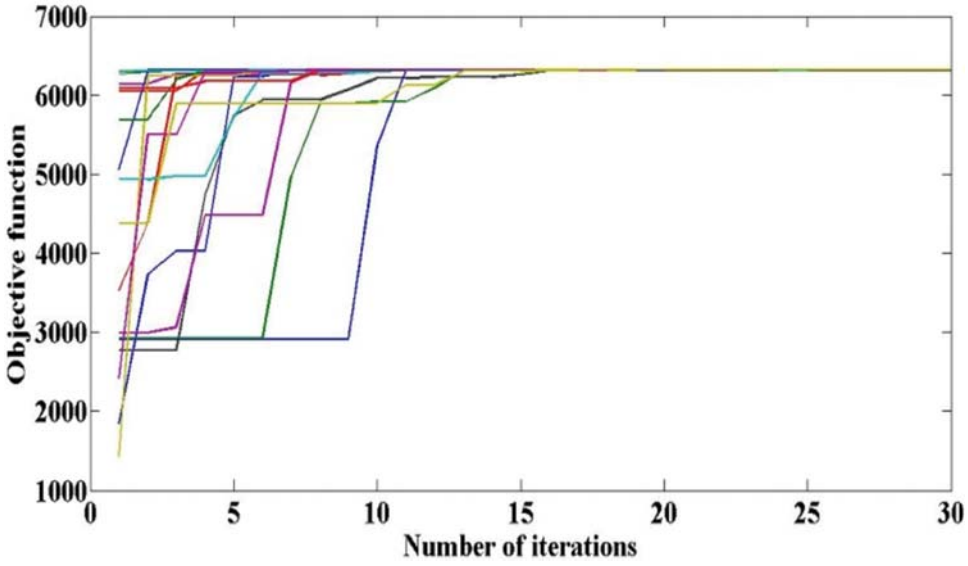

Fig. 7. Convergence graph of ABC based Tsallis algorithm

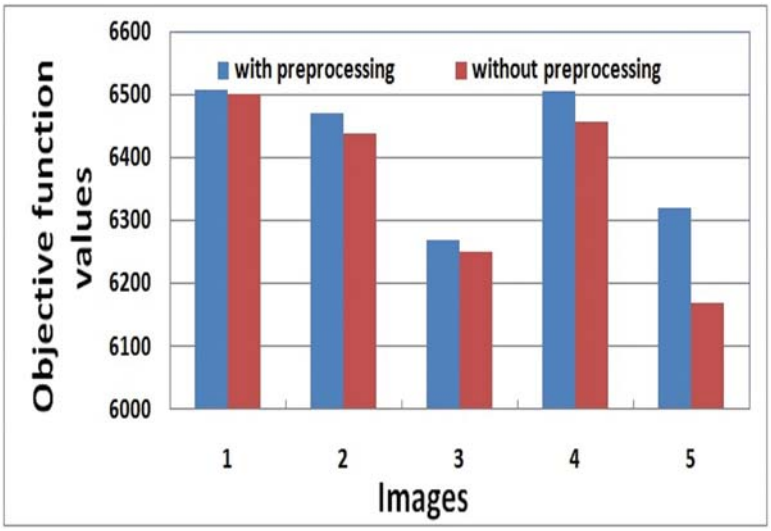

Fig. 8. Variation of objective function values for with and without preprocessing

value provides better threshold values for segmentation. A maximum value of 6506 is observed for image 1 with pre-processing. Marginal difference in objective function values of 6 to a maximum of 150 is observed for images with and without pre-processing. Ground truth generation is not a must, since maximum objective function value signifies the best threshold based on Tsallis algorithm[13]. Moreover objective function value is a quantitative measure. From Fig. 8 it is very evident that, with pre-processing, objective function value has increased which signifies that noise has been reduced.

Fig. 9 shows the variation of entropic index with the objective function for the considered images. It is observed that for 'q' value of 0.2 maximum objective value is obtained. For entropic index value of 1.2 and 2, the cost function drastically reduced to less than 10 which clearly denote that with entropic index value

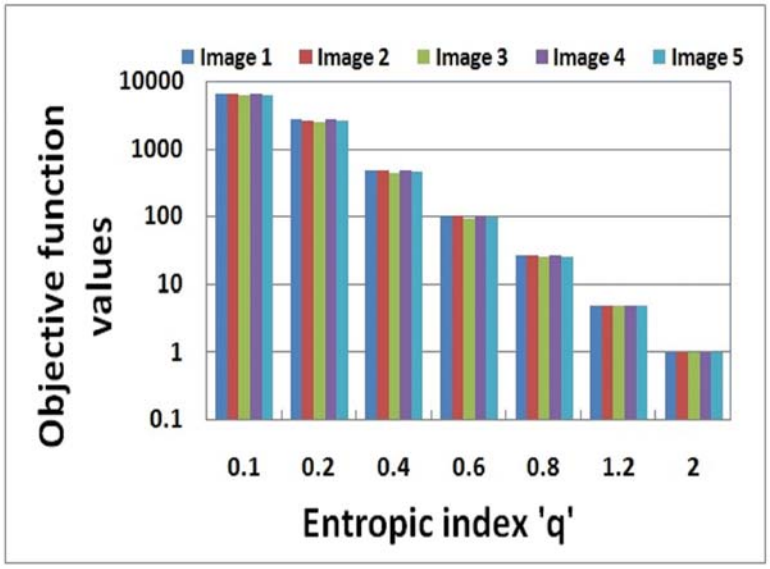

Fig. 9. Variation of entropic index with objective function

of 0.2, better results are achieved. Table - I illustrates the variation of entropic index 'q' and the thres level for the considered images. For 'q' value of 0.1 to 0.8, marginal variation of threshold are observe the entropic index increases beyond 1, the threshold value increases to typical value of 164 and above. threshold increase is clearly reflected in the reduction of objective function values as shown in Fig. 8 fo same entropic index value.

Table 1. Threshold values for various entropic index

Entropic index 'q'	Image 1	Image 2	Image 3	Image 4	Image 5
0.1	127	130	129	130	127
0.2	126	132	128	132	126
0.4	129	137	127	136	128
0.6	130	143	131	139	130
0.8	128	145	130	140	131
1.2	164	169	159	159	137
2	195	192	160	160	169

4. CONCLUSION

In this work, ABC based Tsallis entropy segmentation method is applied for BOSS images. This method is first time implemented and reported for BOSS images. Pre-processing was carried out for images to enhance the contrast using MATLAB function. Bilevel threshold was determined for various 'q' values and threshold values were determined by evaluating an objective function defined in Tsallis entropy method. For entropic index value of 0.1, optimum threshold is determined. A maximum objective function value of 6506 is observed for segmentation with pre-processing method. The objective function values for the images with and without pre-processing are compared. Marginal difference in objective function values of 6 to a maximum of 150 is observed for images with and without pre-processing. From the segmentation results, it is very evident that automatic object detection is achieved by ABC based Tsallis entropy method.

5. ACKNOWLEDGEMENTS

Authors would like to thank the Director, National Institute of Ocean Technology for providing encouragement and permitting to publish the work. Authors acknowledge Marine Sensors Systems team, NIOT for data collection carried out at Royapuram, Chennai, India. The work carried out is funded by Ministry of Earth Sciences, Government of India.

6. REFERENCES

[1] F. Langner, C. Knauer, W. Jans and A. Ebart, 2009. Side Scan Sonar image resolution and automatic object detection, classification and identification, *IEEE Oceans 2009, Europe*.

[2] Hyeonwoo Cho, Son-Cheol Yu, 2015. Real-time sonar image enhancement for AUV-based acoustic vision, *Elsevier Ocean Engineering*, **104**, 568-579.

[3] M.N.V.S.S. Kumar, G. Sasi Bhushana Rao, 2012. A New Image Synthesis Algorithm for Detection of Underwater Objects from Sector Scan SONAR for Navigation of AUV, *International Journal of Graphics & Image Processing*, **2**(3), 211-216.

[4] Jianning Han, Peng Yang and Lu Zhang,2014. Object Recognition System of Sonar Image Based on Multiple Invariant Moments and BP Neural Network, *International Journal of Signal Processing, Image Processing and Pattern Recognition*, **7**(5), 287-298.

[5] Scott Reed, Yvan Petillot and Judith Bell, 2003. An Automatic Approach to the Detection and Extraction of Mine Features in Sidescan Sonar, *IEEE Journal of Oceanic engineering*, **28**(1), 90-105.

Max Mignotee, Christophe Collet, Patrick Pérez and Patrick Bouthemy, 2003. Sonar Image Segmentation Using an Unsupervised Hierarchical MRF Model, *IEEE Transactions on image processing*, **9**(7), 1216-1231.

Xiu-Fen Ye, Zhe-Hui Zhang, Peter X. Liu and Hong-Ling Guan, 2010. Sonar image segmentation based on GMRF and level-set models, *Elsevier Ocean Engineering*, **37**, 891-901.

Guangyu Liu, Hongyu Bian and Hong Shi, 2012. Sonar Image Segmentation based on an Improved Level Set Method, International Conference on Medical Physics and Biomedical Engineering Physics Procedia, **33**, 1168-1175.

[9] Turgay Celik and Tardi Tjahjadi, 2011. A Novel Method for Sidescan Sonar Image Segmentation, *IEEE Journal of Oceanic Engineering*, **36**(2).

[10] Liu Hongpoa, Sun Junb, Wu Haic, Teng Shuhuac and Tan Zhiguoc, 2010. High Resolution Sonar Image Segmentation by PSO based Fuzzy Cluster Method", *IEEE Fourth International Conference on Genetic and Evolutionary Computing*, pp. 18-21.

[11] V. Rajinikanth, J.P. Aashiha and A. Atchaya, 2014. Gray-Level Histogram based Multilevel Threshold Selection with Bat Algorithm, *International Journal of Computer Applications*, **93**(16), 1-5.

[12] Samy Sadek and Ayoub Al-Hamadi, 2015. Entropic Image Segmentation: A Fuzzy Approach Based on Tsallis Entropy, *International Journal of Computer Vision and Signal Processing*, **5**(1), 1-7.

[13] K. Manikantan, B.V. Arun, Darshan Kumar and S. Yaradoni, 2012. Optimal Multilevel Thresholds based on Tsallis Entropy Method using Golden Ratio Particle Swarm Optimization for Improved Image Segmentation, *International Conference on Communication Technology and System Design Procedia Engineering*, **30**, 364 - 371.

[14] Batool Pouryani, Mehdi sadegh zadeh and Seyed Javad Mirabedini, 2014. Seafloor Side scan Sonar Image Segmentation, *International Journal of Mathematics and Computer Sciences*, **29**, 833-847.

[15] Raquel Fandos, Leyna Sadamori and Abdelhak M. Zoubir, 2011. High quality segmentation of synthetic aperture sonar images using the min-cut / max-flow algorithm", *19th European Signal Processing conference, Spain*, pp. 51-55.

[16] Bahriye Akai, 2013. A study on particle swarm optimization and artificial bee colony algorithms for multilevel thresholding, *Applied Soft Computing*, **13**, 3066-3091.

[17] Enfang Sang, Zhengyan Shen, Chang Fan and Yuanshou Li , 2009. "Sonar Image Segmentation Based on Implicit Active Contours", *IEEE 2009, Shanghai China*, pp. 228-231.

[18] Xin-Jiang, Renjie-Zhang and Shengdong-Nie, 2012. Image segmentation based on Level Set Method, *International Conference on Medical Physics and Biomedical Engineering, Physics Procedia*, **33**, 840-845.

[19] Nitin Chamoli, Sneh Kukreja and Monika Semwal, 2014. Survey and Comparative Analysis on Entropy Usage for Several Applications in Computer Vision, *International Journal of Computer Applications*, **97**(16), 1-5.

[20] Suresh Manic, R. Krishna Priya and V. Rajinikanth, 2016. Image Multi thresholding based on Kapur / Tsallis Entropy and Firefly Algorithm, *Indian Journal of Science and Technology*, **9**(12), 1-6.

[21] Vaishali R . Kulkarni and Veena Desai, 2016. ABC and PSO: A comparative Analysis, *IEEE International Conference on Computational Intelligence and Computing Research (ICCIC)*, Chennai, India.

[22] Nida M. Zaitoun and Musbah J. Aqel, 2015. Survey on Image Segmentation Techniques, International Conference on Communication, Management and Information Technology, *Procedia Computer Science*, **65**, 797-806.

[23] Sayanti Bardhan, Mahimol Eldhose, Dhilsha Rajapan, P.M. Rajeshwari, D.S. Sreedev, Shijo Zacharia, C. Kannan, Shibu Jacob and M.A. Atmanand, 2015. "Detection of Buried Objects Using Active Sonar", *IEEE Underwater technology*, pp. 23-25.

[24] U. Anitha and S. Malarkkan, 2015. A Novel Approach for Despeckling of Sonar Image, *Indian Journal of Science and Technology*, **8**(S9), 252-259.

[25] Yan Zhou, Qingwu Li and Guanying Huo, 2105. Automatic Side-Scan Sonar Image Enhancement in Curvelet Transform Domain, *Hindawi Publishing Corporation Mathematical Problems in Engineering*, pp. 1-14.

[26] http://www.mathworks.com

[27] Qianqian Lin and Congjie Ou, 2012. Tsallis entropy and the long-range correlation in image thresholding", *Elsevier Signal Processing*, **92**, 2931-2939.

[28] M. Portes de Albuquerque, I.A. Esquef, A.R. Gesualdi Mello and M. Portes de Albuquerque, 2004. Image thresholding using Tsallis entropy, *Pattern Recognition Letters*, **25**, 1059-1065.

[29] D. Karaboga and B. Basturk, 2008. On the performance of artificial bee colony (ABC) algorithm", *Applied Soft Computing*, **8**, 687-697.

[30] Miao Ma, Jianhui Liang, Min Guo, Yi Fan, and Yilong Yin, 2011. SAR image segmentation based on Artificial Bee Colony algorithm", *Applied Soft Computing*, **11**, 5205-5214.

[31] Yudong Zhang and Lenan Wu, 2011. Optimal Multi-Level Thresholding based on maximum Tsallis Entropy via an Artificial Bee Colony Approach, Entropy, **13**, 841-859.

The Journal of Acoustical Society of India : Vol. 45, No. 3, 2018 (pp. 141-149)

Experimental verification of quadratic chirp detection using modified fractional Fourier transform

G. Sreekumar[1,3], Leena Mary[2] and A. Unnikrishnan[1]
[1]Rajagiri School of Engineering and Technology, Kochi, India
[2]Government Engineering College, Idukki, Kerala, India
[3]Mahatma Gandhi University, Kottayam, Kerala, India
ggsreekumar80@gmail.com

[Received: 20-09-2017; Revised: 15-04-2018; Accepted: 10-05-2018]

ABSTRACT

Detection and parameter estimation of targets using antenna arrays play a significant role in the field of sensor array signal processing. In this paper, the experimental verification of quadratic chirp detection using modified fractional Fourier transform (FrFT) is done by extending the conventional FrFT. As FrFT is limited to the analysis of linear chirps, detection using modified FrFT is found suitable for higher order chirps with the proper selection of the kernel. The parameters of the quadratic signal which construct the kernel is extracted using the polynomial chirplet transform time-frequency distribution method. The effectiveness of the algorithm is validated experimentally for the detection of buried concrete blocks beneath the sea-bed using real data obtained from a practical sonar array as well as using numerical simulations.

1. INTRODUCTION

Chirp signals which exist in either linear or non-linear form are of particular interest in the active and passive systems of radars[1] and sonars[2,3]. The reverberation and the fast fading nature of the underwater channel make it necessary to use chirp waveforms for sonar transmissions. As chirp signals exhibit a change in instantaneous frequency with time, the conventional frequency domain method based on Fourier transform fails to represent. Therefore the concept of time-frequency representation (TFR)was utilized which represents the magnitude of the chirp in both time and frequency domains simultaneously. Short time Fourier transform[4] and continuous wavelet transform[5] are the early published literature on TFRs. However both methods do not guaranty fine resolution in both time and frequency domains on account of the uncertainty principle. To improve the resolution in this regard, Wigner-Ville distribution (WVD)[6] has been proposed. However, WVD exhibits cross terms for multi-component signals due to the product terms in its definition.

Hence efficient and effective concentration of chirp using better methods are needed and fractional Fourier transform (FrFT) stands out as an excellent candidate[7]. The FrFT method is not influenced by cross terms and it decomposes the signal into an orthonormal basis of linear chirps. Also it is highly resistant to noise and promises low computational complexity[8,9]. However the impact of FrFT is restricted to linear chirps as it only rotates the time-frequency plane. Therefore new techniques of TFRs need to be developed for non-linear chirps. Sahay *et al.*[10, 11] introduced the idea of modified FrFT for the analysis of

non-linear chirps. But the parameters of the non-linear chirp, which are large in number based on the chirp order have to be searched for the unknown signal. As these parameters are proportional to the coefficients of the polynomial representing the chirp, the polynomial chirplet transform (PCT)is found to be a good choice[12]. PCT is a modified version of the conventional chirplet transform, which can extract the coefficients of both linear and nonlinear chirps.

2. METHOD AND DATA USED

2.1 Method used

The linear chirp is represented by the equation shown below where b is the chirp rate, f_0 is the start frequency and c is the initial phase of the chirp.

$$s(t) = \exp\left[j2\pi\left(bt^2 + f_0 t + c\right)\right] \tag{1}$$

The term $bt^2 + f_0 t$ + cre presents the instant aneous phase and $2bt + f_0$ defines the instant aneous frequency (IF). Therefore three parameters define a linear chirp completely *viz*. start frequency, chirp rate and the duration over which *'t'* is defined.

The FrFT of a signal *s(t)* is defined as

$$S_\phi(u) = F_\phi\left[s(t)\right] = \int_{-\infty}^{+\infty} K_\phi(t,u)s(t)dt \tag{2}$$

where ϕ is the anticlockwise rotation angle of the transform varying from 0 to $\pi/2$. When $\phi = \pi/2$, FrFT reduces to the classical FT and the inverse FrFT is obtained by substituting $\phi = -\pi/2$. p is the fractional order of FrFT, which can be any real number between 0 and 1 and is related to the rotation angle as $\phi = p\pi/2$. $K_\phi(t,u)$ is the FrFT kernel defined as

$$K_\phi(t,u) = \sqrt{1 - j\cot\phi}\exp\left[j\pi\left(\left(t^2 + u^2\right)\cot\phi - 2tu\csc\phi\right)\right] \tag{3}$$

The relationship between the chirp rate b and the rotation angle ϕ is given by

$$\phi = \tan^{-1}\left(\frac{f_s^2}{2bM}\right) \tag{4}$$

where f_s is the sampling frequency and M is the number of time samples.

The chirp signal represented at its optimum order produces impulses and the theoretical peak point which transforms the natural frequency to fractional frequency is given by

$$u = (f_0 + bT)\sin(\phi) \tag{5}$$

in which T represents the chirp pulse width and the term $f_0 + bT$ defines the mid-frequency of the chirp.

The signal of interest in the present discussion is the quadratic chirp which is represented by the following equation

$$s(t) = \exp\left[j2\pi\left(at^3 + bt^2 + f_0 t + c\right)\right] \tag{6}$$

where a is the additional parameter w.r.t. linear chirp given by (1) which controls the curvature of the quadratic chirp term. Here the IF trajectory of the signal is a non-linear function of time (hence referred to as quadratic) given by

$$f(t) = 3at^2 + 2bt + f_0 \tag{7}$$

The modified FrFT of the quadratic chirp is given by

$$S_{\phi,\psi}(u) = F_{\phi,\psi}[s(t)] = \int_{-\infty}^{+\infty} K_{\phi,\psi}(t,u)s(t)dt \tag{8}$$

where $K_{\phi,\psi}(t,u)$ is the modified FrFT kernel defined as

$$K_{\phi,\psi}(t,u) = \sqrt{1-j\cot\phi}\exp\left[j\pi \begin{pmatrix} \left(t^2+u^2\right)\cot\phi - 2tu\csc\phi \\ -2tu\csc\phi - 2\psi t^3 + 2\psi u^3 \end{pmatrix} \right] \tag{9}$$

The parameters are related to the polynomial coefficients as

$$a = \psi; b = \frac{f_s^2}{2M\tan\phi}; f_0 = u\csc\phi - bT \tag{10}$$

Hence the expression of the modified FrFT of the quadratic signal represented by(6) with zero initial slope is given by

$$F_{\phi,\psi}[s(t)] = \sqrt{1-j\cot\phi}\exp\left[j2\pi\psi u^3 \right] \times \int_{-\infty}^{+\infty} s(t) \times \exp\left[-j2\pi\psi t^3 \right] \exp\left[j\pi\left(\left(t^2+u^2\right)\cot\phi - 2tu\csc\phi\right)\right] dt \tag{11}$$

Therefore the modified FrFT of the quadratic signal involves thefollowing steps.

(i) Multiplication of the quadratic chirp s(t) with exp [-j2π t^3] (another quadratic chirp) which results in a linear chirp to which FrFT can be applied. The evaluation of the FrFT finally result in a function of 'u'.

(ii) Multiplication of the above function in 'u' with another quadratic chirp exp [j2π tu^3].

The chirp parameters ϕ and ψ, which are proportional to the polynomial coefficients are searched over their respective ranges which becomes a tedious process. To avoid the search procedure, the coefficient values are extracted using the PCT approach.

In the PCT based IF estimation method, the polynomial order needs to be assumed at the initial step as there is no prior knowledge about the IF. Usually a large order is adopted at the beginning and if the IF can be well approximated by a low order, then the estimated higher order coefficients would be close to zero. Then the PCT is obtained with the coefficients all set to zero in the beginning to roughly estimate an IF. Then the roughly estimated IF is approximated using a polynomial function by the least square method. Again PCT is performed with the new polynomial kernel for the given signal. Therefore by adjusting the polynomial kernel using the IF obtained from the PCT and performing the PCT again using the new polynomial kernel, better refinement in IF is observed. Finally the IF of the signal can be visualized from the TFR produced by the PCT [12].

2.2 Data used

2.2.1 Simulated signals

A single transmitted quadratic chirp given by (12) with f_0 = 3000 Hz and b = 2500 Hz/s is reflected from multiple moving targets located at different positions

$$s(t) = \exp\left[j2\pi\left(10t^3 + 2500t^2 + 3000t\right)\right] \tag{12}$$

The chirp signal undergoes a shift in the frequency band due to Doppler effect[9] and the reflected chirps are shown by (13-15).

$$s_1(t) = \exp\left[j2\pi\left(10t^3 + 2515t^2 + 3020t\right)\right] \tag{13}$$

$$s_2(t) = \exp\left[j2\pi\left(10t^3 + 2533t^2 + 3040t\right)\right] \tag{14}$$

$$s_3(t) = \exp\left[j2\pi\left(10t^3 + 2550t^2 + 3061t\right)\right] \tag{15}$$

The frequency shifts are found to be different when using the Doppler equation for the three moving targets with velocities 5, 10 and 15 m/s. The same rotation angle was retained for the reflected chirps as the shift in the bandwidth was observed only within 6 to 20 Hz. But due to the shift in the frequency band, the bin values get shifted for the received chirps as shown in Figure 1 and Figure 2 for SNR = 0 dB and SNR = -10 dB respectively. Three distinct peaks in the modified FrFT domain are observed as given by Figure 1 (b) and Figure 2 (b) which correspond to the three active moving chirp targets with overlapping frequency bins. This results in the resolution of the closely spaced quadratic chirp sources using modified FrFT approach even at very low SNR.

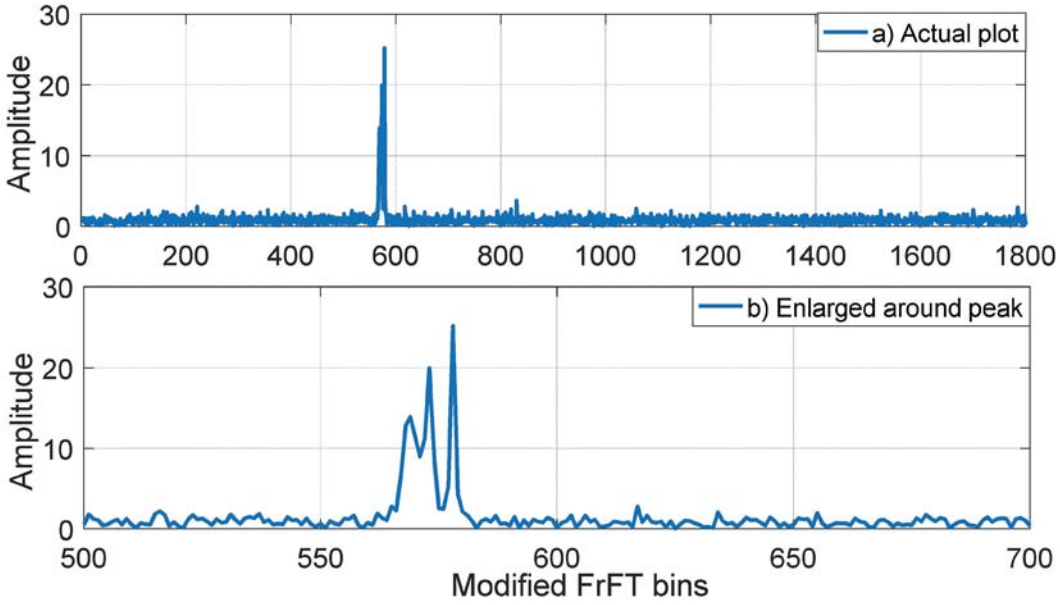

Fig. 1. Modified FrFT detection of multiple moving active chirp targets for SNR = 0 dB. (a) Actual plot (b) Enlarged in and around the peak

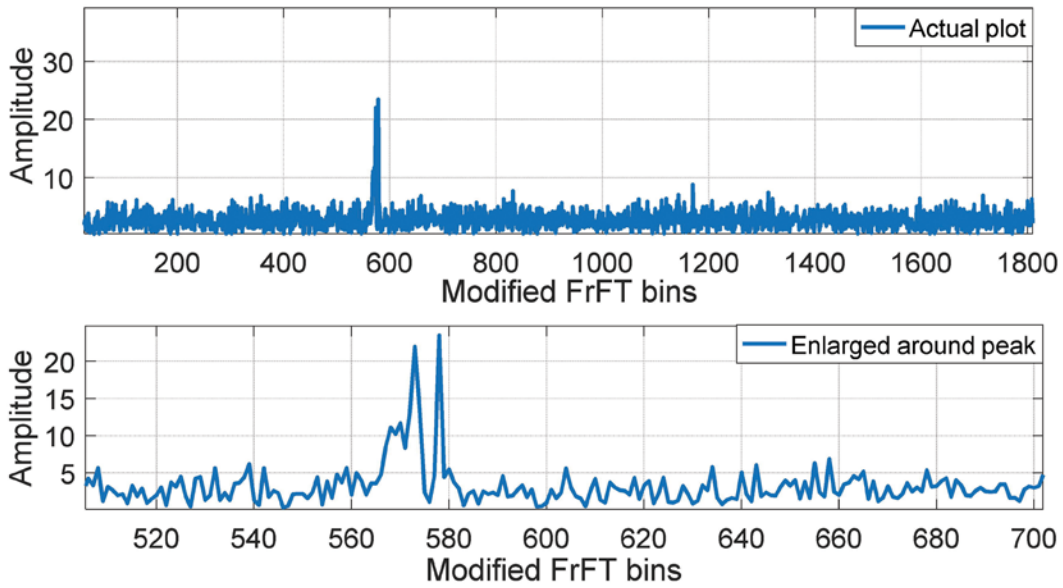

Fig. 2. Modified FrFT detection of multiple moving active chirp targets for SNR = -10 dB. (a) Actual plot (b) Enlarged in and around the peak.

2.2.2 Real data using sonar array

The transmitted signal is shown in Figure 3 (a) below, which is a Blackman-Harris modulated linear chirp signal of 3 ms duration having the frequency range of 2-24 kHz. The transmitter is driven by a 200 W linear power amplifier and is transmitted at 4 pings / s interval. The reflected signals are acquired by eight linear hydrophone array elements with a sampling frequency of 100 kHz. The inter-element spacing between each hydrophone in the array is 0.0325 m. The whole system called Buried Object Detection Sonar(BODS) for finding targets in the seabed has been developed by National Institute of Ocean Technology (NIOT), Chennai, India and is mounted in floating tow body having a speed range of 1-3 m / s[13].

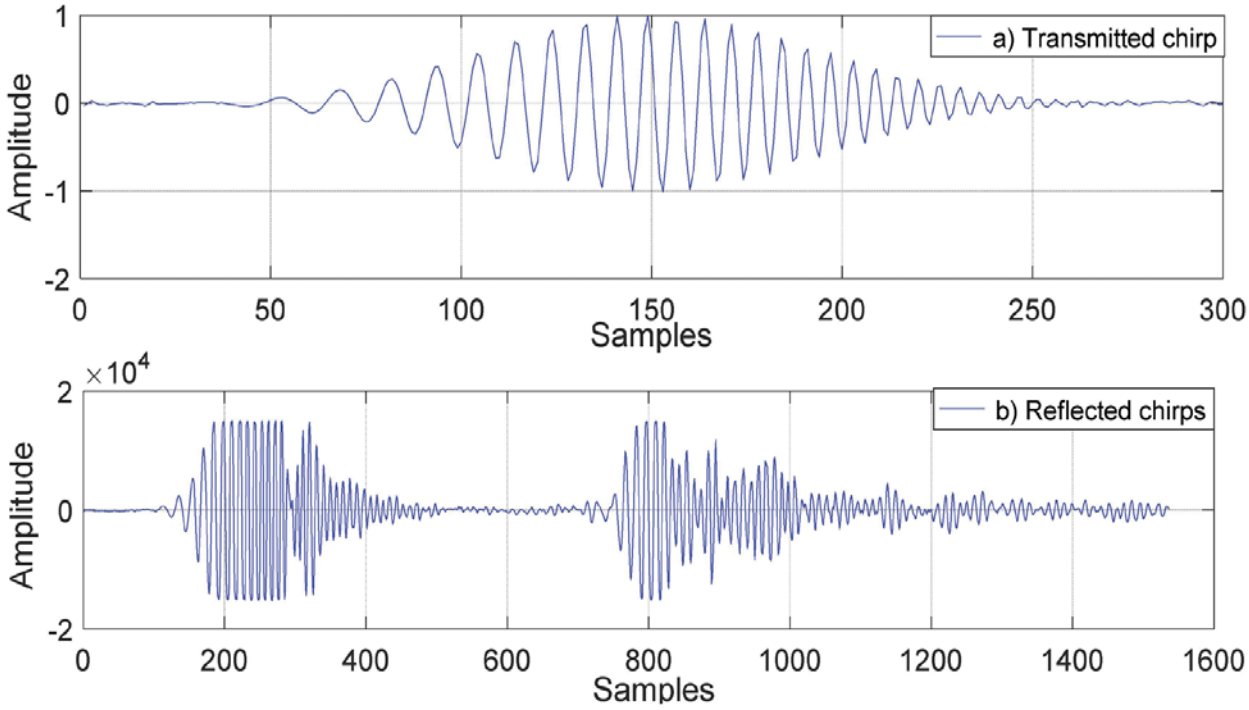

Fig. 3. (a) Transmitted chirp (b) Series of reflected chirps acquired using one of the hydrophones in the array.

The sea trial for testing the BODS system with buried objects was performed at Royapuram Harbor, Chennai, India. A water column depth of 4.5 to 5 m was available at the site. The sediment type at the site was clay mixed with sand and concrete blocks were selected to be buried at the test site about 0.47 m in the seabed. Twenty concrete blocks are arranged in five rows and four columns, where each block has a dimension of 0.3 m × 0.3 m × 0.02 m, hence the entire concrete block set is of the dimension l.5 m × l.2 m × 0.02 m. The raw data from each channel corresponds to 1536 samples which altogether make 1536 × 8 samples.

Figure 3(b) shows the series of reflected chirps acquired using one of the hydrophones in the array. As the transmitted chirp penetrates into the water column it gets reflected first by the air-water interface, then by the mud layers in the sea-bed and finally by the buried objects beneath the sea-bed. To separate these chirps, a joint time-frequency representation (TFR) based on polynomial chirplet transform (PCT) is employed. Fig 4 shows the TFR of the raw data using PCT approximation with a third order fit. Two strong reflections are marked in the plot, of which one is the reflection from the air-water interface and the other from the concrete blocks.

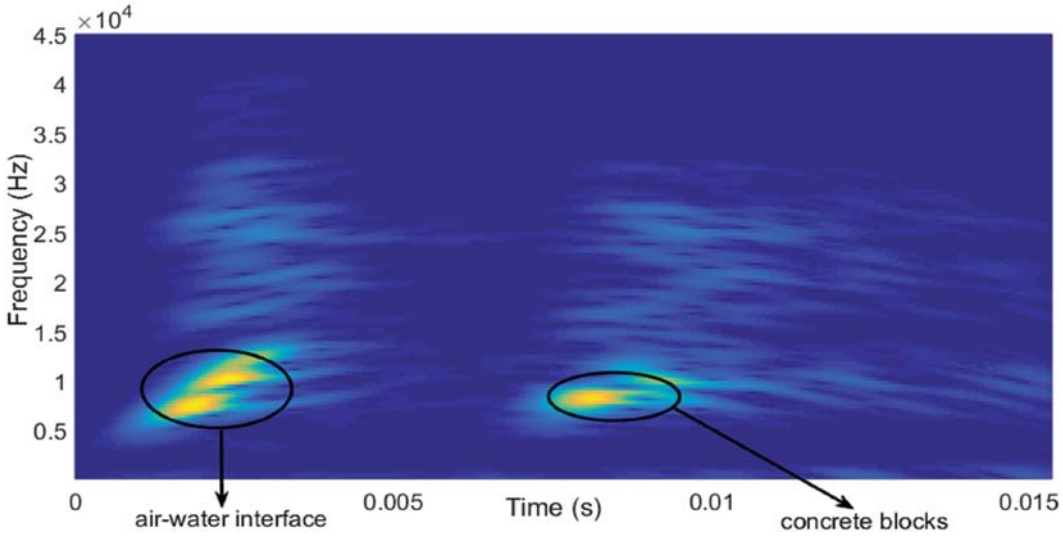

Fig. 4. Joint time-frequency representation based on polynomial chirplet transform for the reflected chirp.

3. RESULTS AND DISCUSSIONS

The detailed analysis of reflected chirps obtained from air-water interface and concrete blocks are shown in Figure 5 and Figure 6 respectively. The figures also include the comparison of modified FrFT detection with the conventional FrFT and FFT methods. Figure 5(a) represents the TFR peak data of the reflected chirp from air-water interface using PCT after fourth iteration. It is clear from the plot that the response is non-linear even though the transmitted chirp was linear. This is due to the absorption of the high frequency

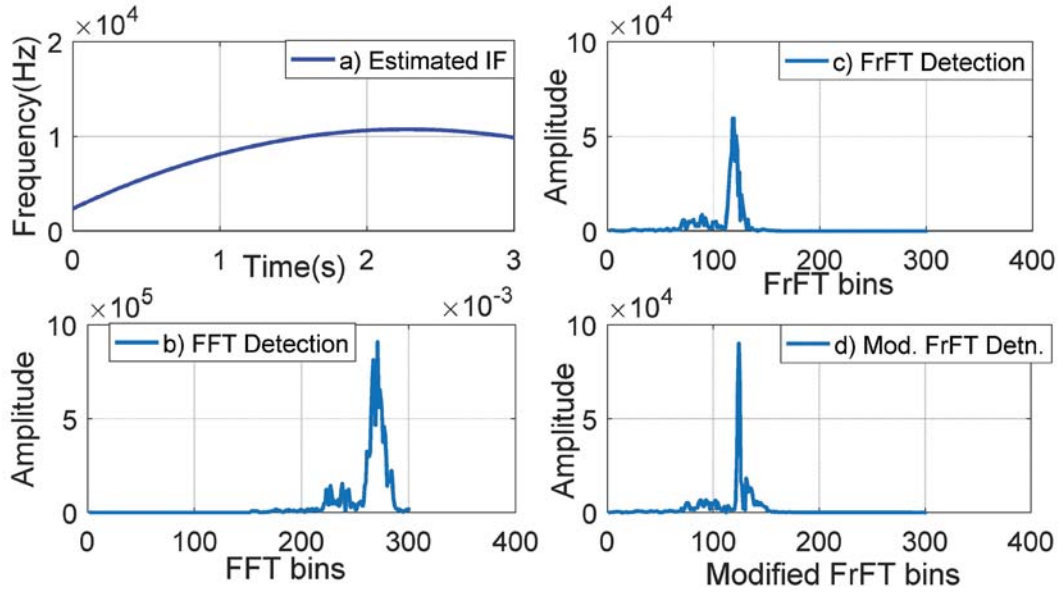

Fig. 5. Detection of back reflected signal from air-water interface obtained using sonar array. (a) Estimated IF for the reflections from air-water interface (b) Detection of the reflected chirp using FFT method (c) Detection of the reflected chirp using FrFT method (d) Detection of the reflected chirp using modified FrFT method.

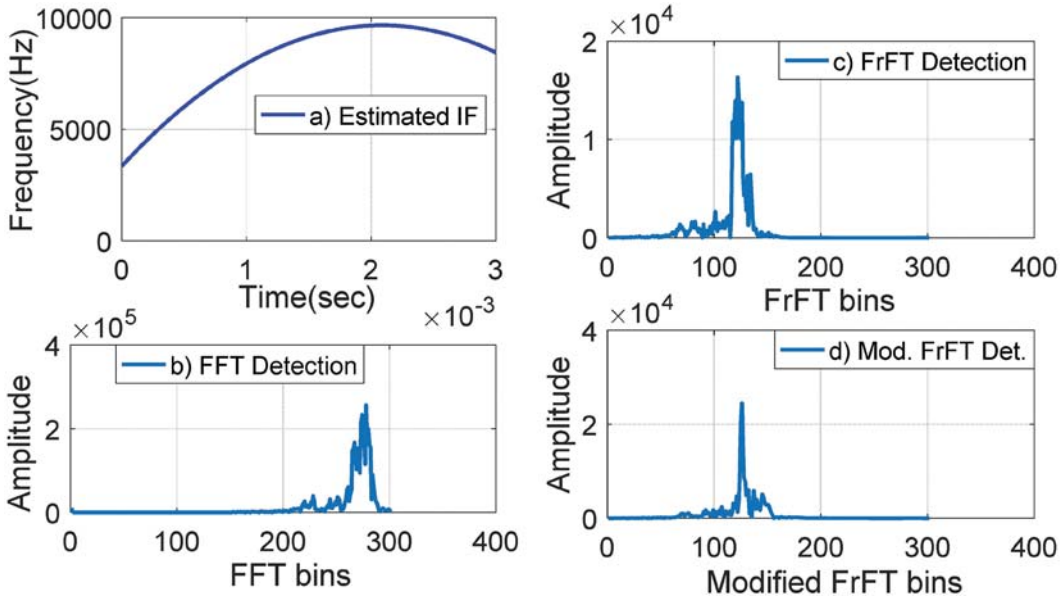

Fig. 6. Detection of back reflected signal from concrete blocks obtained using sonar array. (a) Estimated IF for the reflections from concrete blocks (b) Detection of the reflected chirp using FFT method (c) Detection of the reflected chirp using FrFT method (d) Detection of the reflected chirp using modified FrFT method.

Table 1. Estimated coefficients using third order polynomial chirplet transform for the concrete reflections

Coefficients	**1**	**2**	**3**	**4**
a	6223	5549	5160	5008
2b	3265564	5086915	6066146	6483634
3c	-318555610	-1278732825	-1797243811	-2023053641

contents by the medium and the reflected chirp falls in the frequency range of 5 kHz to 10 kHz within a time gap of 1.5 ms. Table 1 also strengthens the above fact which represents the estimated coefecients using third order PCT approximation. The last column shows the polynomial coefecients after fourth iteration and the IF given by $a + 2bt + 3ct^2$, comes to 10 kHz where t = 1.5 ms.

The high frequency data which falls in the time period of 1.5 ms to 3 ms in the transmitted chirp is no longer reflected back from the medium. The main cause of sound attenuation in sea water at high frequencies is due to the viscosity phenomenon. Figure 6(a) represents the TFR peak data of reflected chirp from concrete reflections using PCT, which again result in a non-linear curve similar to Figure 5(a). Here also the high frequency components are seen absorbed by the medium. Also the bending of frequencies at higher depth is observed in Figure 6(a) compared to Figure 5(a) between 2 to 3 ms. This is due to the reduction in bandwidth with increased transmission range. Based on the under water reflections, the channel can therefore be modelled as a series of band-pass filter for low frequencies and a series of notch filter at high frequencies.

Due to the non-linearity in the received data, detection using modified FrFT has to be performed which results in a peak value as given by Figure 5(d) and Figure 6(d) respectively for air-water interface and concrete reflections. The conventional FrFT method of detection given by Figure 5(c) and Figure 6(c) for air-water interface and concrete reflections respectively cannot result in a single peak. Therefore it is turned out that conventional FrFT method of detection, which is suitable only for linear chirp data doesn't holds good for underwater applications. The FFT method of detection, shown in Figure 5(b) and Figure 6(b) is not at all a good candidate for any chirp detection owing to the instantaneous frequency nature of the chirp.

Likewise the detection of all quadratic chirps displayed in the time-frequency plot can be obtained. Moreover, the depth of the object can be visualized from the time-frequency plot using conversion of time information to distance. More research in this direction can lead to better object classification and underwater imaging as compared to the conventional FFT matched filtering type.

4. SUMMARY AND CONCLUSION

In this paper, the efficacy of applying modified FrFT to the detection of quadratic chirps is presented in detail. FrFT has great potential in sonar signal processing over the conventional Fourier transform detection as it takes advantage of the knowledge of transmitted waveform. The parameters of the quadratic chirp is extracted using polynomial chirplet transform time-frequency distribution method. This also improves the computational efficiency with respect to the existing system employing brute-force search.The performance of the algorithm has been tested over a large range of SNR and compared with the traditional methods using simulated data as well as real data obtained from a practical sonar array. Beam-forming using modified FrFT would help to further improve the detection performance. Moreover the detection using different FrFT variants can be extended to other practical chirps such as exponential chirps.

5. ACKNOWLEDGEMENTS

The authors would like to thank Dr. M. A. Atmanand, Director - NIOT and Marine Sensor Systems group for sharing the data set. We also would like to thank the authors of[12] for sharing their Matlab code, which we used to produce the results shown in Figures 5(a) and 6(a).

6. REFERENCES

[1] M.A. Richards, 2005. Fundamentals of radar signal processing, *McGraw-Hill*.

[2] S. Zhou and P. Willett, 2007. "Submarine location estimation via a network of detection only sensors," *IEEE Trans. Signal Process.*, **55**(6), 3104-3115.

[3] G. Sreekumar, Leena Mary and A. Unnikrishnan, 2018. "DoA estimation of broad-banded linear and quadratic chirps using nested and co-prime arrays," *Int. Jour. of Computer Sciences and Engineering*, **6**(7), 49-57.

[4] B. Boashash, P.J. O'Shea and M.J. Arnold, 1990. "Algorithms for instantaneous frequency estimation: A comparative study," in Proc. SPIE: Advanced Signal-Process. Algorithms, Architectures and Implementations, San Diego, **1348**, 126-148.

[5] R.A. Scheper and A. Teolis, 2003. "Cramer Rao bounds for wavelet transform based instantaneous frequency estimates," *IEEE Trans. Signal Process.*, **51**(6), 1593-1603.

[6] L.J. Stankovi, I. Djurovi and R.M. Lakovi, 2003. "Instantaneous frequency estimation by using the Wigner distribution and linear interpolation," *IEEE Trans. Signal Process.*, **83**(3), 483-491.

[7] Namias, 1980. "The fractional order Fourier transform and its application to quantum mechanics," *J. Inst. Math. Appln.*, **25**, 241-265.

[8] R. Jacob, T. Thomas and A. Unnikrishnan, 2009. "Applications of fractional Fourier transform in sonar signal processing," *IETE Jour. Res.*, **55**, 16-27.

[9] G. Sreekumar, Leena Mary and A. Unnikrishnan, 2018. "Performance Analysis of Fractional Fourier Domain Beam-Forming Methods for Sensor Arrays," *Smart Science Jour., Taylor and Francis publication*.

[10] S. Sahay, D. Pande, V. Gadre and P. Sohani, 2012. "A novel generalized time frequency transform inspired by the fractional Fourier transform for higher order chirps," *International Conf. on Signal Process. (SPCOM).*

[11] S. Sahay, T. Meghasyam, Rahul K. Roy, G. Pooniwala, S. Chilamkurthy and V. Gadre, 2015. "Parameter estimation of linear and quadratic chirps by employing the fractional Fourier transform and a generalized time frequency transform," *Sadhana,* **40**(4), 1049-1075.

[12] Z.K. Peng, G. Meng, Z.Q. Lang, F.L. Chu, W.M. Zhang and Y. Yang, 2011. "Polynomial chirplet transform with application to instantaneous frequency estimation," *IEEE Trans. Meas. and Instrum*. **60**(9), 3222-3229.

[13] S. Bardhan, D. Rajapan, S. Zacharia, M. Eldhose, P.M. Rajeshwari, D.S. Sreedev, C. Kannan , S. Jacob and M.A. Atmanand, 2015. "Detection of buried objects using active sonar," *(IEEE-UT 15).*

The Journal of Acoustical Society of India : Vol. 45, No. 3, 2018 (pp. 150-158)

Performance analysis of coding techniques in underwater acoustic communication

K. Chithra, Tata Sudhakar and M.A. Atmanand
National Institute of Ocean Technology, Chennai-600100, India
chithra@niot.res.in

[Received: 20-09-2017; Revised: 15-04-2018; Accepted: 10-05-2018]

ABSTRACT

For any wireless communication channel coding is an essential requirement. Achieving high performance wireless underwater communication with frequency selective fast fading channel is challenging. Performance of the communication system can be enhanced by including efficient Forward Error Correction (FEC) coding / decoding techniques. Performance of various channel coding techniques mitigating the underwater channel effects are discussed in the paper. Linear Block coding along with interleaving is a simple coding technique. Complex coding technique, Convolutional coding with various constraint lengths and Viterbi decoding techniques are implemented and performance comparison of the coding techniques are discussed in detail. Block Interleaving, spreading the coded data in both frequency and time domain resulted in significant Bit Error Rate reduction. The implemented coding technique was tested in a sea trial experiment and the results are presented.

1. INTRODUCTION

Having wide application in oceanography, marine research, defense and offshore systems, underwater communication is one of the potential areas for research recently. This attention comes from potential applications of such channel including sharing of navigation information, control of autonomous underwater vehicles (AUV) and undersea command and control. Standard acoustic channel model doesn't exist yet[2]-[4] because of the complex ocean environment characteristics. Attaining high data rate in underwater wireless communication is challenging due to time and frequency spreading, high frequency absorption, low frequency ambient noise, limited bandwidth and propagation delay[5]. Also requirements arise to meet high data rate for video / picture communication and hence research continues to improve underwater communication performance as in[6]-[8]. For a communication scheme with suitable modulation technique, Channel coding improves transmission reliability by protecting the information from channel impairments. Compared to Automatic Repeat Request (ARQ), Forward Error Correction (FEC) is adopted in real-time Communication system where the information must be protected on one-way channel and critical delay control is required. Based on the underwater channel parameters, performance of various coding schemes has been investigated. Orthogonal Frequency Division Multiplexing (OFDM) Modulation technique with Quadrature Phase Shift Keying (QPSK)[1] is the modulation technique adopted for the communication scheme. Block Coding with linear and block interleaving, Convolutional coding of various constraint lengths with Viterbi decoding technique along with block interleaving are compared. Most of the existing literature on OFDM based underwater communication focuses mostly on simulation based studies and conceptual

system analysis. Also many Underwater Acoustic communication schemes are examined by offline data processing based on recorded experimental data. Such methods may fail in receiver processing real-time detection. The shortcoming based on the recent literature survey led to addressing the real-time system for performance analysis of communication system.

2. UNDERWATER COMMUNICATION CONSTRAINTS

Time varying multipath : The major factor characterizing underwater acoustic channel is Time varying multipath propagation. The travel distance, propagation loss and reflection loss encountered by each path is different. Arrival of acoustic signal from all these paths causes attenuation and time spreading. Frequency dependent path loss induced by the refection loss also results in time spreading. If each path delay is represented by τ_p (t) and the attenuation encountered in the path, α_p (t), then the cumulative channel impulse response is represented by Eq. (1) [9],

$$g(\tau;t)=\sum_p \alpha_p(t)\delta\left[t-\tau_p(t)\right] \tag{1}$$

The physical geometry of sea surface and sea bed is random and complex in nature and the motion of the transducers due to sea surface motion and ocean current is unpredictable. Hence both τ_p(t) and α_p(t) can be expressed as random process. The received signal y(t) through the channel for a transmitted signal x(t), can be represented by Eq. (2) [9],

$$y(t)=x(t)*g(\tau;t)+n(t)=\sum_p \alpha_p(t)x\left[\tau-\tau_p(t)\right]+n(t) \tag{2}$$

Where, *n(t)* is the additive background noise. The underwater acoustic channel is time-varying frequency selective because of the time and frequency dispersion.

Doppler Spread: The movement between the transmitter and the receiver and the time varying dynamic motion of the medium result in frequency spreading of the underwater channel. Doppler spread is caused due to the random motions of sea surfaces and currents[9]. Each arrival ray contributes Doppler shift due to the relative motions between the transmitter and receiver. Doppler shifts caused by these rays are different since their arriving angles are different resulting in Doppler spread. The receiver system should be capable of compensating the resultant Doppler spread.

In underwater acoustic propagation, attenuation increases with frequency and hence acoustic propagation is best supported at low frequencies. Since attenuation increases with frequency, for long range communication low frequency band only can be used, this in turn reduces the channel capacity. Channel capacity of multi carrier system given by Eq. (3),

$$C_{N_c}=\sum_{n=0}^{N_c-1}\log(1+\frac{\mathrm{P_n}\mid \mathrm{h_n}\mid^2}{\mathrm{N_0}}) \tag{3}$$

Bandwidth is extremely limited for long range communication. Attenuation grows with frequency where as noise decays with frequency, resulting in a signal-to-noise ratio (SNR) that varies over the signal bandwidth. The Signal-to noise ratio for a band of frequency around the frequency *f* at a distance *l*, can be expressed as in Eq. (4),

$$\mathrm{SNR}(l,f)=\frac{\mathrm{S}_l(f)}{A(l,f)N(f)} \tag{4}$$

Where, $S_l(f)$ is the power spectral density function of the transmitted signal, $A(l,f)$ is the attenuation function and $N(f)$ is the noise function. It is evident that SNR is a function of frequency for any given distance.

Background noise or the ambient noise is another parameter that deteriorates the performance of underwater communication. Noise domination is more in low frequencies and decays with increase in

frequency. Underwater acoustic propagation speed is low, ~1500 m/s, which limits the use of Automatic Repeat Request (ARQ) for error monitoring and correction through repetition of transmission for real-time communication.

3. ERROR CONTROL CODING

A system with transmitting capability R_s bits/sec if coded with code rate R_c, where $R_c = k/n$, for k source bits and n coded bits, requires increase in transmitting capability by a factor R_s/R_c bits/sec. Bandwidth required also must be increase by $1/R_c$ factor [15]. It is evident from the fact that by using channel coding bandwidth efficiency decreases by a factor $1/R_c$ compared to uncoded transmission. Also if same transmission time is considered for coded and uncoded symbols, each binary encoded symbol mapping duration $T_c = R_c/R_s$ seconds is shorter than that used in the uncoded by a factor R_c. With E_b the energy per unit bit and assuming same transmitting power, coding decreases the energy per channel bit to the value E_bR_c. As a result more channel bits will be incorrectly demodulated than with uncoded transmission. Though these observations about coding are discouraging, a well designed coding/decoding system will compensate for the large number of errors during decoding by the error correcting capabilities of the decoder. An efficient coded communication system should cater for overall error performance for the same or better bandwidth efficiency using the same or reduced transmission power. The achievable reduction in the required transmitting power for a coding system is referred to as coding gain. Coded systems are performance evaluated based on the attained coding gain. Coding gain is measured as the difference (in decibels) in the required value of SNR to achieve a given bit error probability between uncoded and coded systems. For low values of SNR there can be a crossing between the coded and uncoded curves, meaning that the coding gain becomes negative. In other words, there is a limit to what a code can do in terms of improving a bad channel. Fig. 1. shows the basic block diagram of a coded communication system.

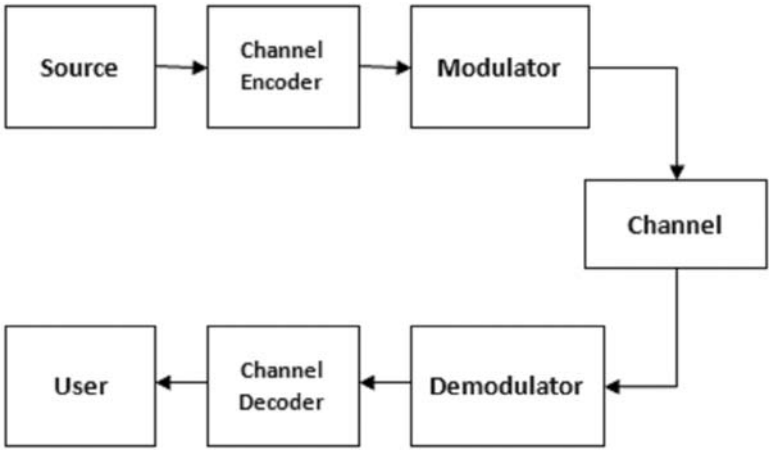

Fig. 1. Communication Scheme employing Channel Coding

3.1 Forward Error Correction (FEC) Coding

The reliability of the information transmitted through the communication channel is enhanced by the Forward Error Correction Coding/Decoding techniques. These are techniques to control the error probability based on addition of redundancy to the information sequence. Though the name 'error correcting coding', error in the binary sequence entering the decoder may not be corrected by the decoder but the decoder estimates the probable transmitted information sequence. FEC leads to code gain thereby reducing the transmission power requirement of the digital communication system for a given noise level. Jamming margin can be increased by using a suitable FEC technique in spread spectrum communication system.

3.2 Choice Of Coding Parameters

Application of FEC coding in the communication scheme and the choice of coding parameters are influenced by various factors. Effect of physical communication channel witnesses isolated, random errors and burst errors in some channels. Modulation technique employed and the required rate of information transmission are some other issues. Use of redundancy information calls for larger bandwidth is tolerable due to enhancement in system performance. Large code length FEC technique with good error correcting capability and high data rate demands complex hardware / software. FEC offers different coding gain for different code rates.

3.3 Block Code

Block of *n* bits is generated by the encoder using a procedure from the corresponding block of *k* information bits. Such a block coding is referred as *(n, k)* code. A block of bits are encoded at a time and hence the block encoder is memoryless. Hamming distance between 2 code words is the number of bit positions in which the two code words differ. The smallest among the hamming distances between distinct code words is called the minimum distance d_{min} of the code.

A linear block code *(n, k)* with minimum distance d_{min} can detect all error vectors of weight not greater than (d_{min}-1) and correct all error vectors containing no more than (d_{min}-1) / 2 errors. Block codeword polynomial is given in Eq. (5) - Eq. (8),

$$m(x) = \mathrm{m}_0 + m_1 x + m_2 x_2 + \ldots + m_{k-1} x_{k-1} = \sum_{i=0}^{k-1} m_i x_i \tag{5}$$

$$c(x) = \sum_{i=1}^{n-1} c_i x^i = \mathrm{c}_0 + \mathrm{c}_1 \mathrm{x} + \mathrm{c}_2 \mathrm{x}^2 \ldots + \mathrm{c}_{n-1} \mathrm{x}^{n-1} \tag{6}$$

$$g(x) = \sum_{i=0}^{n-k} \mathrm{g}_i \mathrm{x}^i = \mathrm{g}_0 + \mathrm{g}_1 \mathrm{x} + \mathrm{g}_2 \mathrm{x}^2 \ldots \mathrm{g}_{n-k} \mathrm{x}^{n-k} \tag{7}$$

$$c(x) = m(x).g(x) \tag{8}$$

where, *m(x)* is the message polynomial, *g(x)* is the generator polynomial and *c(x)* is the codeword polynomial.

3.4 Convolutional Coding

Convolutional codes differ from block codes in terms of their structure, design tools and analysis. Block codes are based on Combinatorial / algebraic techniques whereas convolutional codes are based on construction techniques. Good convolutional codes can be found from the sequential state machine nature of convolutional encoder rather than from the algebraic properties of the code like in block code. Convolutional encoder is an encoding system with memory. Convolutional encoder, unlike block encoders, encodes the entire data stream into a single codeword, regardless of its length, by convolving a sequence of information bits with 'generator' sequences and multiplexing operations. Data stream need not be segmented into blocks of fixed size in Convolutional coding.

Convolutional code is specified by *(k/n, K)* where, k is the input, n is the output and *K* is the constraint length for encoder with *(K-1)* memory elements. Coding rate, *k/n* specifies number of data bits per coded bits. Fig 2. depicts the convolutional encoder for 1 / 2 code rate with constraint length *K*=3 using generator polynomial (7, 5).

The encoding operation of a single input encoder can be represented as follows.

$$Y^i(D) = X(D) G_j^{(i)}(D) \tag{9}$$

$$Y^{(i)}(D) = [X(D)] \begin{bmatrix} G_0^{(0)}(D) & G_0^{(1)}(D) & \cdots & G_0^{(n-1)}(D) \\ G_1^{(0)}(D) & G_1^{(1)}(D) & \cdots & G_1^{(n-1)}(D) \\ \vdots & \vdots & \ddots & \vdots \\ G_{k-1}^{(0)}(D) & G_{k-1}^{(1)}(D) & \cdots & G_{k-1}^{(n-1)}(D) \end{bmatrix} \tag{10}$$

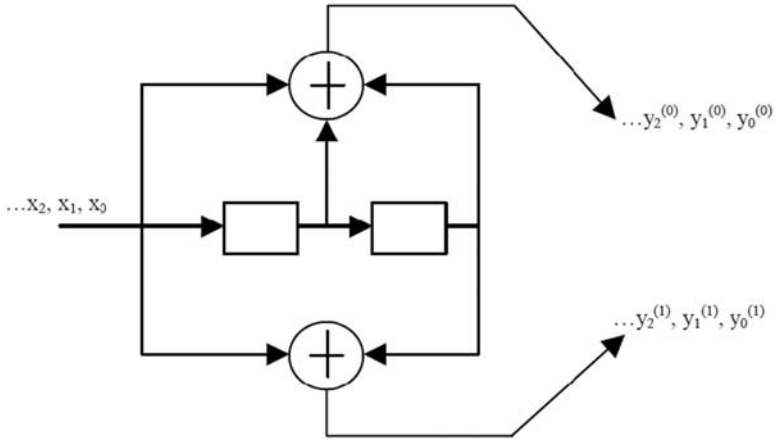

Fig. 2. Convolutional Encoder (1/2, 3)

X(D) and *Y(D)* are delay transforms of input and output respectively. The matrix *G(D)* is called the transfer-function matrix. The number of rows represents the *k* input streams and the number of columns represents the *n* output streams.

4. INTERLEAVING / DE-INTERLEAVING

A random error correcting code along with a suitable interleaver / de-interleaver pair is a robust practical technique to deal with burst errors. An Interleaver rearranges the ordering of bit sequence in a deterministic manner and the de-interleaver applies the inverse operation to restore the bit sequence to its original ordering. The basic communication scheme employing Interleaver / De-Interleaver pair to enhance performance in burst error channel is shown in Fig 3.

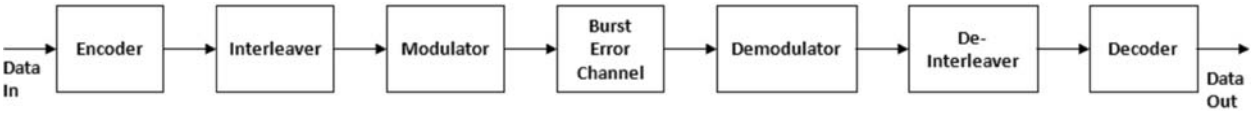

Fig. 3. Communication scheme with Interleaver / De-Interleaver pair for Burst error channel

5. SIMULATION RESULTS

For a communication scheme with suitable modulation technique, Channel coding improves transmission reliability by protecting the information from channel impairments. Orthogonal Frequency Division Multiplexing (OFDM), a multi-carrier modulation technique has many advantages to be applied in highly dispersive underwater channel and is suitable for achieving high data rate in frequency selective underwater channels. Recent researches reveal application of OFDM for underwater acoustic communication for high data rate with improved bit error rate performance [10-14]. OFDM with Quadrature Phase Shift Keying (QPSK) is the modulation technique adopted for the communication scheme. OFDM basic functional blocks are depicted in Fig 4.

Block Coding: A linear code, Walsh-Hadamard code is used to map data of length *'n'* to codewords of length 2^n. All the codes are orthogonal to each other. This code is unique in the sense the hamming weight of each non-zero codeword is 2^{n-1} which ensures code distance also to be 2^{n-1}. 16 bit block coding with 1/4 code rate and interleaving has been used. Code gain of ~5 dB was attained in the simulation result. Performance comparison of block coded system with that of uncoded system is shown in Fig 5.

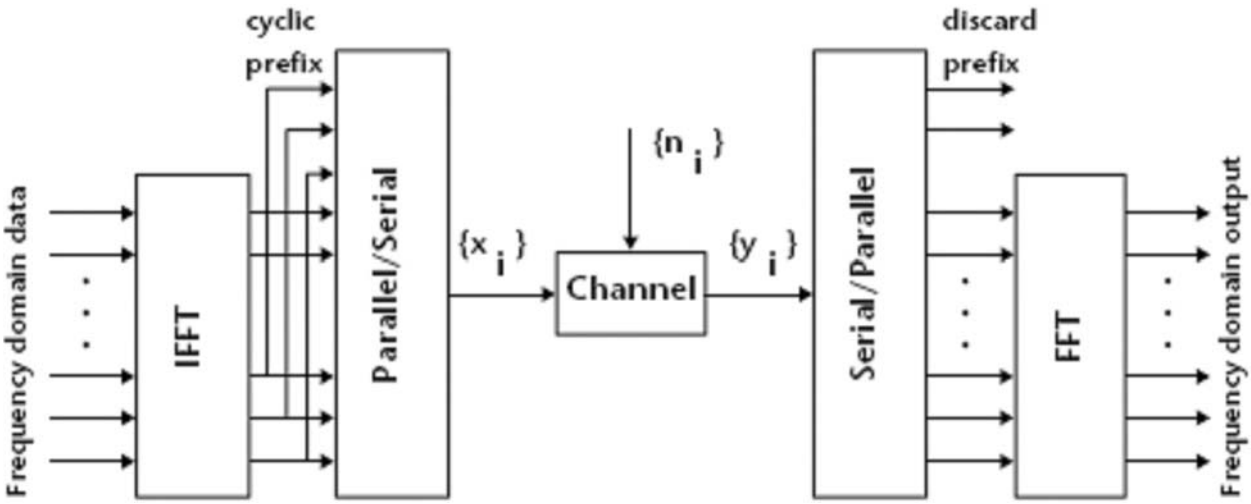

Fig. 4. OFDM Functional Blocks

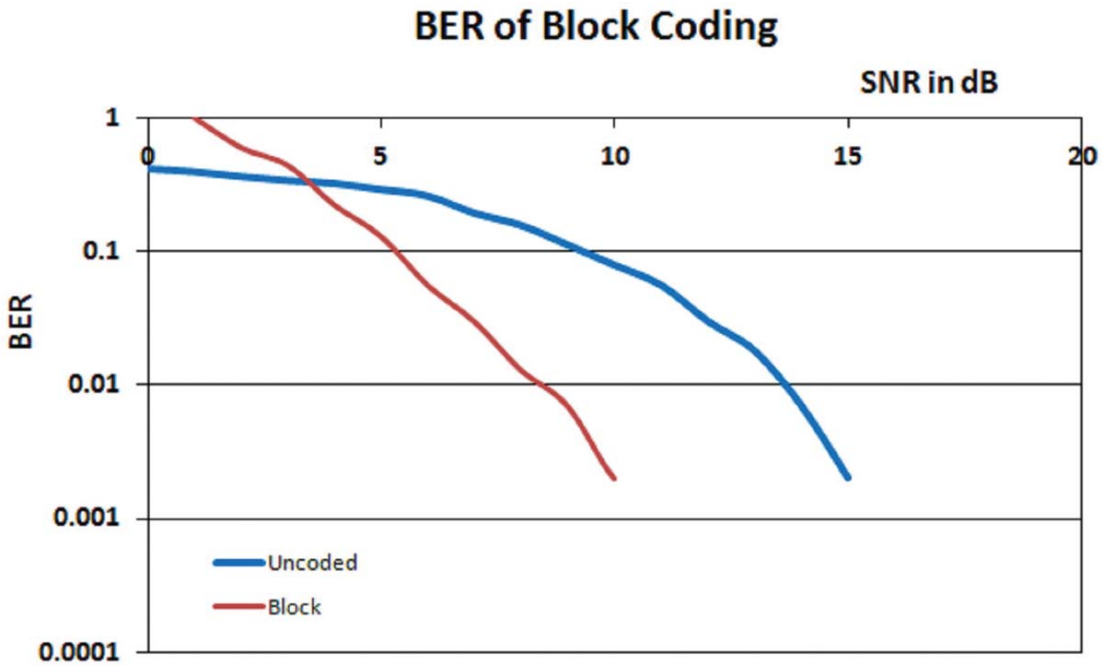

Fig. 5. Performance Comparison of Block coding with Uncoded transmission

Convolutional Coding: Given the decoding requirement of a communication system appropriate bound on K should be determined first and then upper bound on the required data rate is determined. For the specific constraint length and data rate, suitable generator polynomial producing large free distance can be fixed. Accordingly in Convolutional Coding for constraint length *K*=3 generator polynomial (7, 5) was chosen, for constraint length *K*=5, generator polynomial (36, 25) was chosen and for constraint length *K*=7 generator polynomial (133, 171) was chosen. Viterbi decoding technique was adopted in the receiver side. Convolutional coding of various constraint lengths along with viterbi decoding performance is compared with that of uncoded system as shown in Fig 6.

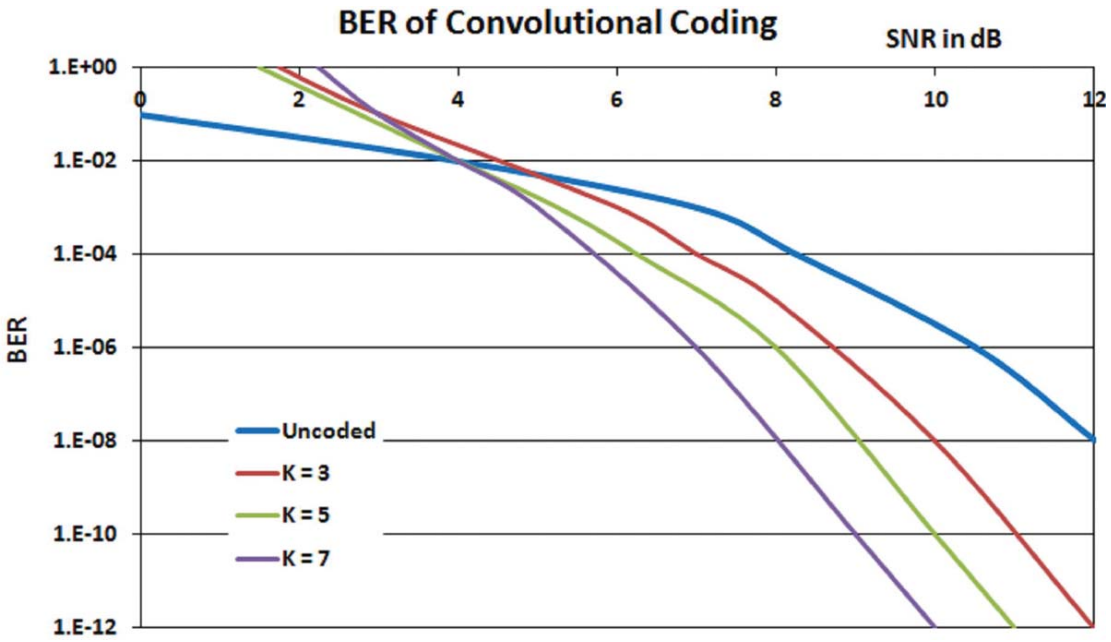

Fig. 6. Performance Comparison of Convolution coding with Uncoded transmission

6. EXPERIMENTAL RESULTS

An open ocean experiment was conducted in Bay of Bengal using a research vessel with the Prototype Acoustic Modem units. The modem units were developed based on OFDM modulation technique employing Convolutional coding with Viterbi decoding technique and Block Interleaving / De-Interleaving. The transducers used for the experiment is ITC3013 capable of both transmitting and receiving with operating frequency 12.5 kHz and 2 kHz bandwidth. The communication performance was tested in the open ocean vertical environment. The transmitter and the receiver were separated ~1100m vertical range in the open ocean environment. The receiver was held from the surface ship at 15m depth. Transmitter was lowered from the ship to 1100m vertically downwards using deep sea winch. Data frame of 1024 bits was transmitted every 5 seconds by the transmitter and receiver retrieved and checked for bit errors. The entire frame consists of 32 symbols and pilot carriers blocks. Pilot carriers were inserted in between the data streams for channel estimation. The frame arrangement is shown in Fig 7 [1]. Out of 36 kbits transmitted 3 errror bits found resulting in BER 0.008%. Fig 8. depicts the typical frame signal received from 100m depth and the constellation plot of the retrieved signal.

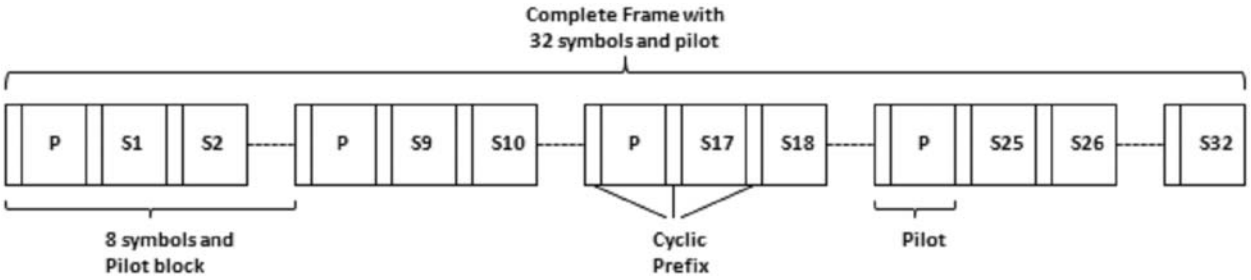

Fig. 7. Frame Arrangement

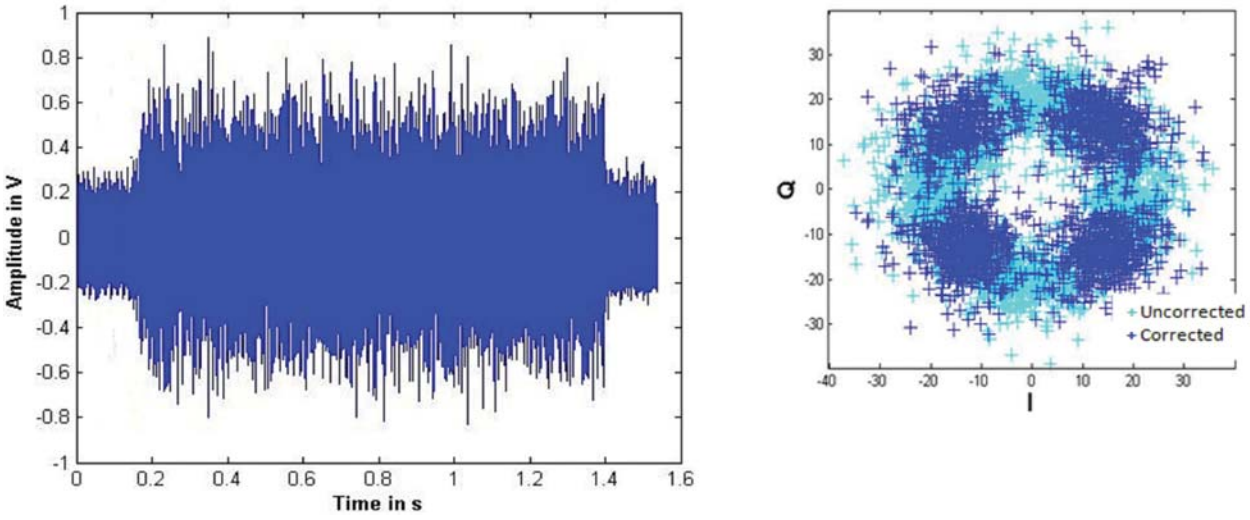

Fig. 8. Frame signal received from 100m depth and the constellation plot of the retrieved signal

7. CONCLUSION

OFDM with QPSK modulation scheme along with coding techniques have been analysed. Code gain, the possible gain in SNR attained for a given Bit error rate (BER) and possible data rate, the effective information rate resulting with redundant bits inclusion are generally the major metrics of interest for any coding technique. The coding technique chosen as a function of the channel's parameters should compromise on both these metrics. Different underwater acoustic channel parameters should be considered for evaluation of coding techniques. Block codes with 1/4 code rate along with Interleaver resulted in better coding gain but with reduction in data rate and easy implementation. Convolutional coding with 1/2 code rate with constraint lengths K=3 (7,5), K=5 (36, 25) and K=7 (133, 171) along with Block interleaver yield ~1 dB coding gain improvement on each case but with increased implementation complexity.

8. ACKNOWLEDGEMENTS

Authors gratefully acknowledge the funding agency, Ministry of Earth Sciences, India and National Institute of Ocean Technology (NIOT) for their support in carrying out this work successfully.

9. REFERENCES

[1] K. Chithra, N. Sireesha, C. Thangavel, V. Gowthaman, S. Sathya Narayanan, Tata Sudhakar and M.A. Atmanand, 2015. "Underwater Communication Implementation with OFDM", *Indian Journal of Geo-Marine Sciences,* **44**(2), 259-266.

[2] P. Hursky, M.B. Porter and M. Siderius, 2006. "Point-to-point underwater acoustic communications using spread-spectrum passive phase conjugation," *Journal of the Acoustical Society of America*, **120**(1), 1-11.

[3] P.A. Walree, 2013. "Propagation and scattering effects in underwater acoustic communication channels," *IEEE Journal of Oceanic Engineering*, **38**(4), 614-631.

[4] M. Stojanovic, 2006. "Underwater wireless communications: current achievements and research challenges," *IEEE Oceanic Engineering Society Newsletter,* **41**(1), 10-13.

[5] A.C. Singer, J.K. Nelson and S.S. Kozat, 2009. "Signal processing for underwater acoustic communications," *IEEE Communications Magazine,* 47(1), 90-96.

[6] Q. Song and M. Garcia, 2012. "Cooperative OFDM underwater acoustic communications with limited feedback: part I," *International Journal of Computer Applications*, **54**(16), 42-46.

[7] H. Esmaiel and D. Jiang, 2013. "Review article: multicarrier communication for underwater acoustic channel," *Communications, Network and System Sciences,* **6**, 361-376.

[8] K. Tuy, D. Fertonani, T. Duman, M. Stojanovic, J. Proakis and P. Hursky, 2011. "Mitigation of intercarrier interference for OFDM over time-varying underwater acoustic channels," *IEEE Journal of Oceanic Engineering,* **36**(2), 156-171.

[9] B-C. Kim and I-T. Lu, 2000. "Parameter study of OFDM Underwater Communications System," in *Proc. IEEE Oceans'00 Conf.*

[10] C. Polprasert, J. Ritcey and M. Stojanovic, 2011. "Capacity of OFDM Systems over Fading Underwater Acoustic Channels," *IEEE Journal of Oceanic Engineering,* **36**(4).

[11] M. Stojanovic, 2008. "OFDM for Underwater Acoustic Communications: Adaptive Synchronization and Sparse Channel Estimation," in *Proc. International Conference on Acoustics, Speech, and Signal Processing (ICASSP'08).*

[12] M. Stojanovic, 2006. "Low complexity OFDM detector for underwater acoustic channels," *IEEE Oceans Conference*.

[13] B. Li, S. Zhou, M. Stojanovic, L. Freitag, J. Huang and P. Willett, 2007. "MIMO-OFDM over an underwater acoustic channel," in *Proc. IEEE OCEANS*, DOI: 10.1109/OCEANS.2007.4449296.

[14] B. Li, S. Zhou, M. Stojanovic, L. Freitag and P. Willett, 2008. "Multicarrier communication over underwater acoustic channels with nonuniform Doppler shifts," *IEEE J. Ocean. Eng.,* **33**(2) 198-209.

[15] Sergio Benedetto, Ezio Biglieri, 1999. "Principle of Digital Transmission with Wireless Applications", Kluwer Academic/Plenum Publishers.

The Journal of Acoustical Society of India : Vol. 45, No. 3, 2018 (pp. 159-164)

Sound wave propagation analysis in an acoustic tank

A. Malarkodi[1], G. Latha[1] and B. Jothi[2]
[1]National Institute of Ocean Technology, Pallikaranai, Chennai-600 100
[2]Vels University, Pallavaram, Chennai-600 117
malar@niot.res.in

[Received: 20-09-2017; Revised: 15-04-2018; Accepted: 10-05-2018]

ABSTRACT

This paper describes the comparative study of sound wave propagation in the acoustic tank with different liner materials by numerical simulation. Simulation carried out for sound wave propagation analysis in a concrete acoustic tank with and without liners such as carbon fiber and rubber materials. The acoustic tank along with the Omni directional source is Modeled and simulated. The analysis was done with spatial and spectral variability ie) the sound pressure level (SPL) at various measurement locations within the acoustic tank for the frequency range from 2 kHz to 20 kHz with different source intensities. The same simulation procedures were carried out for the concrete acoustic tank with carbon fiber and rubber liners separately. The SPL values with three boundaries such as concrete tank, carbon fiber and rubber liners were compared and presented. The simulation is also validated with the experiment data for the concrete boundary.It is observed that the simulation results are close to the results obtained from experiment. The analysis also reveals that the reflected sound signal is attenuated more for carbon fibre liner when compared to the rubber liner.

1. INTRODUCTION

Underwater acoustic tanks are commonly used for underwater electro acoustic transducer calibration and acoustic characterization of hydrophones. It has several advantages as cost efficient and controlled environment, when it is compared with open water environment such as open ocean and lake. However, due to limited tank volume and dimensions, low frequency range of measurement is affected. A possible solution may be to develop methods for underwater transducer characterization taking into account the reverberant field originated in the tank, but these methods are unable to solve source directivity[1]. In order to perform measurements without undesirable reflections from boundaries, it is necessary to make the walls of the tank as well as its bottom and surface, reflection less. To achieve this one needs a broad band absorber, corresponding to the dimensions of the tank, which causes sufficiently small reflections in the desired frequency range. Anechoic materials can have simple and multilayer absorbers, wedge shaped designs, resonant and cavity approaches. Every propagation medium is characterized by its density ρ and the speed of sound c in the medium. It can be interpreted as a measure of how hard it is for sound to propagate in the medium. In general, sound wave propagating through a medium of impedance $Z_1 = \rho_1 c_1$ and encountering an interface with the second medium of impedance $Z_2 = \rho_2 c_2$ are partly reflected off and partly refracted inside the medium[2]. The reflection coefficient that determines the fraction of the sound wave energy reflected back into medium 1 is derived as[3].

$$R = \frac{Z_2 \cos\theta_i - Z_1 \cos\theta_t}{Z_2 \cos\theta_i + Z_1 \cos\theta_t}$$

Where θ_i is the angle of incidence of the wavefront on the interface between the first and second medium, and θ_t is the angle of refraction inside the second medium. The value -20 $\log_{10}$ R(in dB) is called echo reduction, and conveys the capability of the material to attenuate echoes originating from the interface. Several types of materials can be employed as liner materials for acoustic tank. The difference among them is made based on their density. The porous material has the density less than 1 g.cm^{-3}, which is typically employed for sound damping in air as their impedance adapts well to the air's impedance[4]. There are several materials absorb acoustic energy by transforming it into heat through elastic deformation. Compact rubbers, high density polyurethane and carbon fiber present this characteristic behavior as their acoustic impedance adapted to that of water. Compact, polyurethane-based tiles that achieve a broad band echo reduction and absorption are presented[5]. The tiles are well matched to the water impedance, and sound energy absorption is enhanced through the insertion of air micro-spheres and high-density fillers, and by shaping the material in cones. The theory of sound propagation in poro-elastic media was first introduced by Biot in a series of classic papers[6-10]. In this work, the acoustic tank with liner materials along with monopole sound source is modeled for acoustic propagation study. The model was created using the finite element simulation software Comsol Multi physics[11].

2. MODELING AND SIMULATION

Initially the trapezoidal concrete tank was modeled[11] as solid domain and the required water medium was modeled as fluid domain with proper material properties such as density, speed of sound, young's modulus and Poisson's ratio (Figure 1). The monopole sound source was considered and placed exactly at the center of the tank in all the 3 directions (x, y, and z). The material is assigned as PZT (Lead Zirconium Titanate). The fluid model chosen was linear elastic model with appropriate attenuation coefficient. Setting up the boundary conditions is much more important for sound wave propagation analysis. The concrete tank walls are set to sound hard boundary and the top surface of water is set to sound soft boundary (Figure 2). Simulation was carried out for the source pressure of 20Pa and 40Pa with and without liner materials.

Acoustic liners of 50mm thickness used for rubber and carbon fibre materials. Simulation was carried out for the sound propagation of frequency range from 2 kHz to 20 kHz with the source pressure level of 20 Pa and 40 Pa respectively. For simulation SPL are measured at 6 locations within the tank, three in the right side ie) $M_{1(R)}$, $M_{2(R)}$ and $M_{3(R)}$ respectively of the source and three are in the left side of the source

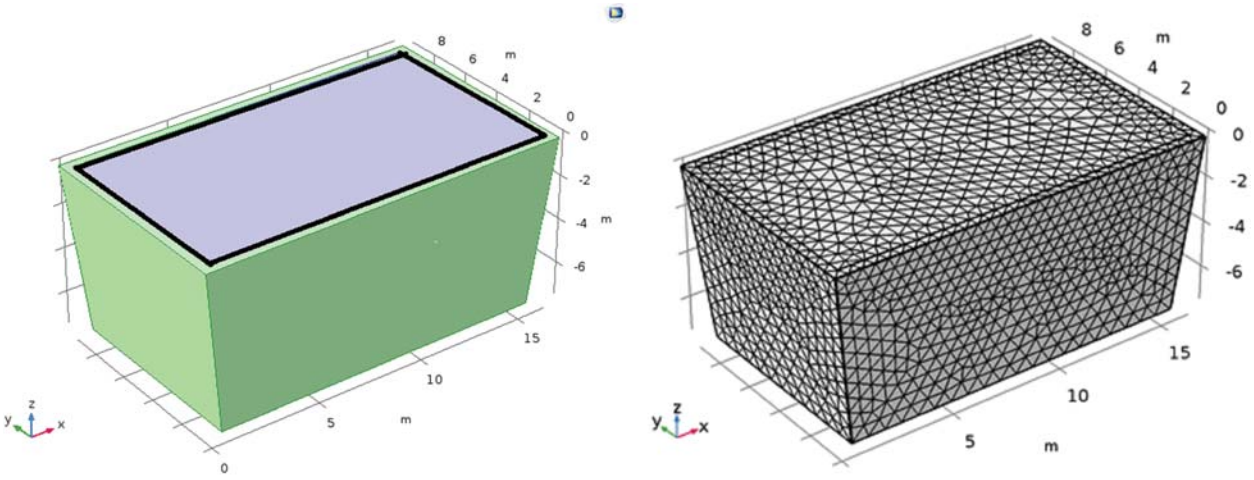

Fig. 1. Model of Acoustic tank with liner material

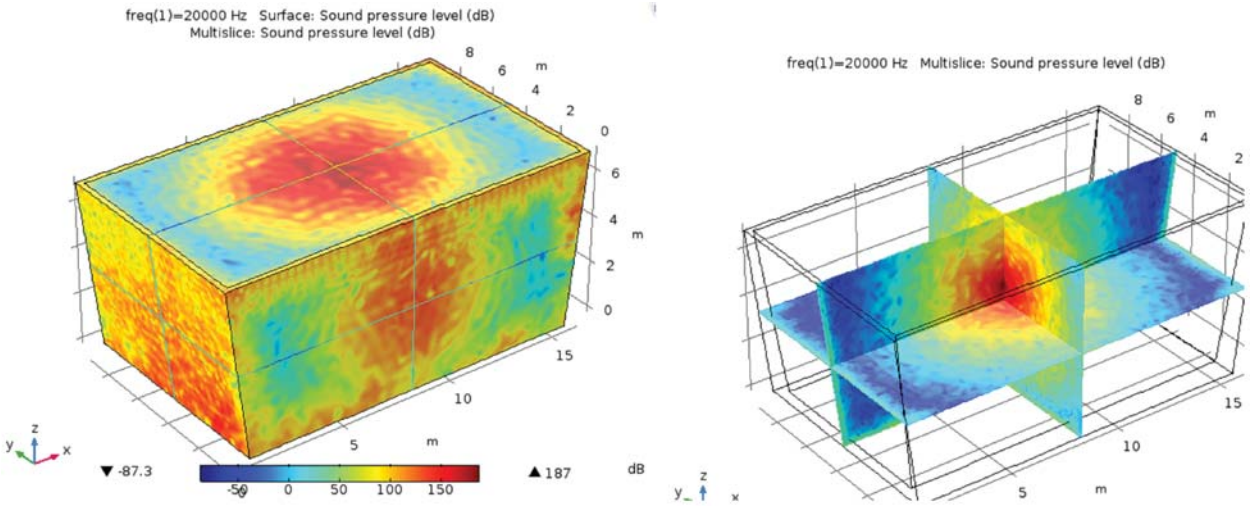

Fig. 2. SPL for 20kHz with multi-slice

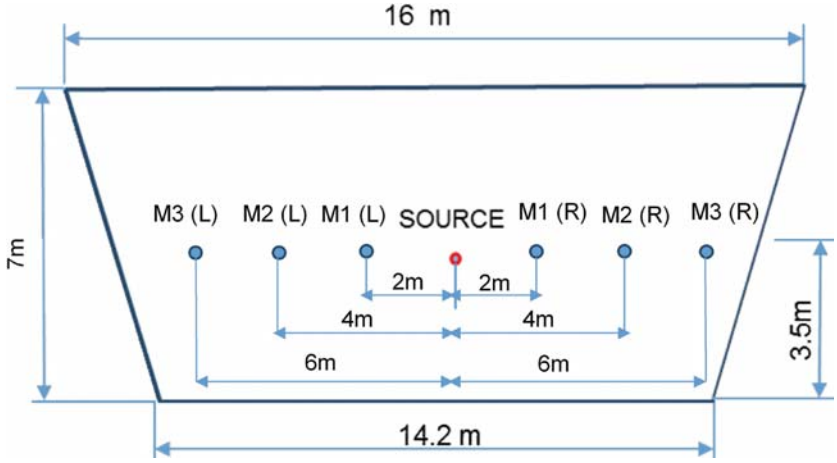

Fig. 3. Source receiver locations in Acoustic Tank

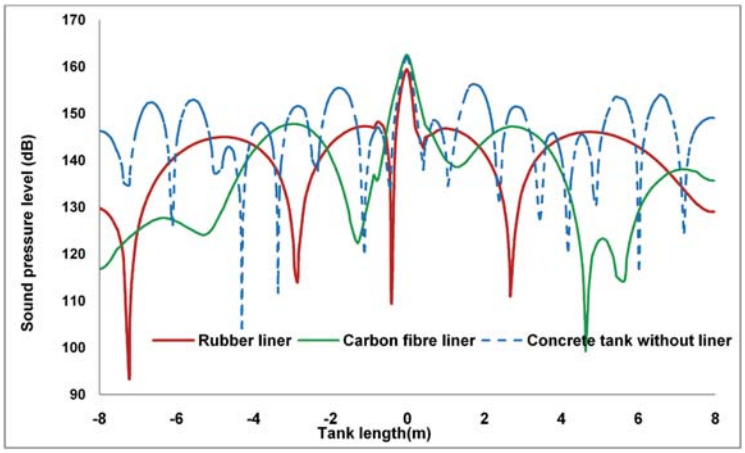

Fig. 4. Comparison of SPL @10kHz with and without liners

position ie) $M_{1(L)}$, $M_{2(L)}$ and $M_{3(L)}$ as shown in Figure 3. The sound propagation simulation was carried out for each frequency from 2 kHz to 20 kHz with and without carbon fiber and rubber liner material.

The SPL values are taken from every locations as mentioned in Figure 2 and are compared. The comparison of SPL with and without carbon fiber liner is shown in Figure 4. This figure illustrate that the reflections are reduced due to carbon fiber liner.

3. EXPERIMENTAL VALIDATION

The results obtained by simulation were validated for concrete tank. Hydrophones of make / models B&K 8103 and Reson TC 4033 used for acquiring signal generated by source transducer of type Neptune sonar D11. The generated signal was amplified and transmitted by the source transducer. Every time the toned burst sine signals are generated continuously and allowed the tank for full reverberation. The source acoustic pressure of 20 Pa and 40 Pa maintained with the continuous sine wave. The receiver hydrophone B&K 8103 fixed at left hand side of the source transducer whereas the TC 4033 positioned right hand side. Location1 ie) $M_{1(L)}$ and $M_{1(R)}$ measured initially and later the acquisition carried at M_2 and M_3 locations (Refer Figure 5). The hydrophone output voltage was measured initially and converted as a sound pressure level by using the sensitivity of the hydrophone at each frequency. For low frequency measurement ie) for less than 5 kHz conditioning amplifier is used to amplify the signal. Both left and right positions are measured simultaneously. Figure 6 illustrate that the comparison of simulation output at $M_{1(L)}$, $M_{1(R)}$ for 20Pa pressure level with experimental results in $M_{1(L)}$.

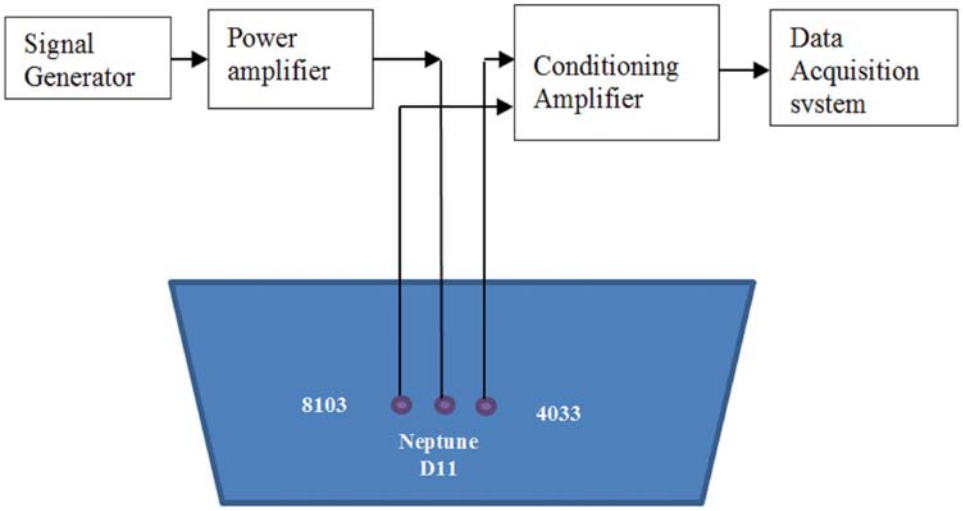

Fig. 5. Experimental setup

4. CONCLUSION

The acoustic tank with omni directional source transducer was modeled with appropriate material properties. Later the acoustic tank with liner materials of rubber and carbon fibre was modeled and used for simulation. The simulation was carried out with spatial and spectral variability ie) the sound pressure level was acquired and compared for the frequency range of 2 kHz to 20 kHz with different positions of the tank. This procedure is followed for the concrete acoustic tank with carbon fiber and rubber liners separately. For validation, the experiment was conducted in acoustic tank and the results are compared with the simulation of concrete boundary. It appears that the results of simulation are close to the results obtained from experiment. Hence it can be expanded this to other problems such as open sea sound wave propagation and underwater acoustic scattering.

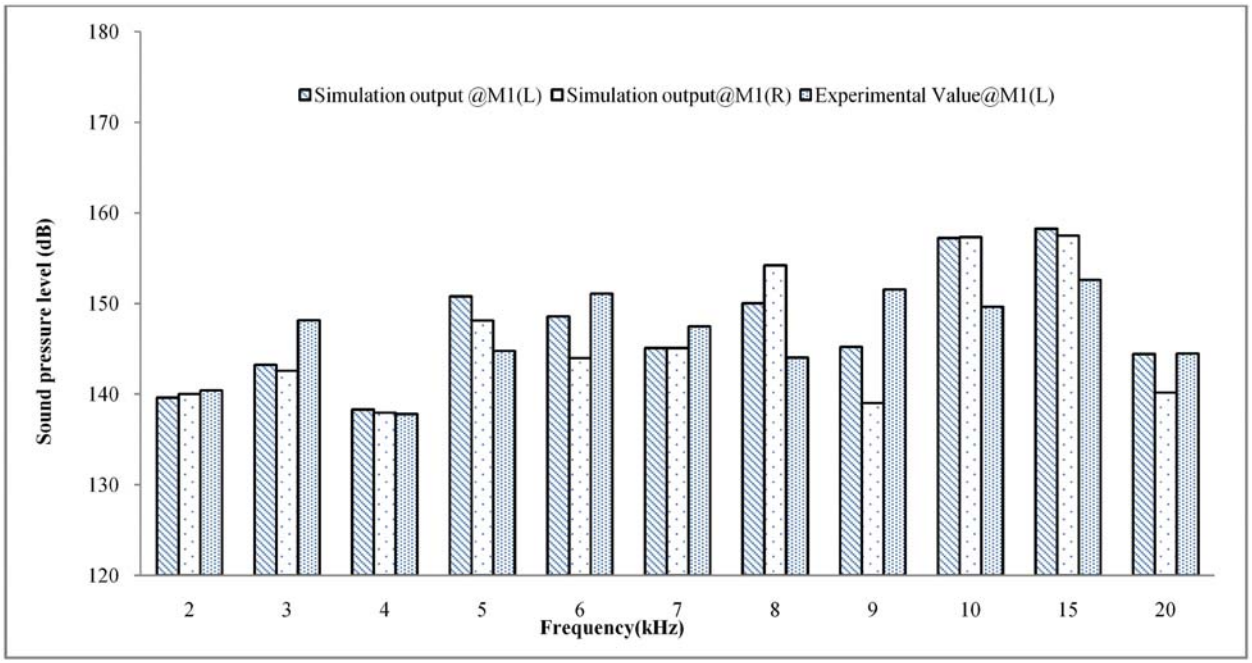

Fig. 6. Comparison of simulation results for 20Pa at $M_{1(L)}$, $M_{1(R)}$ with experimental value at $M_{1(L)}$

5. ACKNOWLEDGEMENTS

The authors would like to express their sincere thanks to the Ocean Acoustics department of National Institute of Ocean Technology for their extensive support and guidance to execute this work. We are very grateful to the Ministry of Earth Sciences, Government of India for funding this project. The authors would also like to acknowledge the team working in Acoustic Test Facility for conducting experiments for validation of simulation results.

6. REFERENCES

[1] N. Cochard, J. Lacoume, L. Arzelies and Y. Gabillet, 2000. Underwater Acoustic Noise Measurement in test tank, *IEEE J. Ocean Engg.*, **25**(4), 516-522.

[2] R.J. Urick, 1983. Principles of underwater sound, *McGraw-Hill.*

[3] L.E. Kinsler and A.R. Prey, 1962. Fundamentals of Acoustics, *John Wiley and Sons, Inc., New York.*

[4] Francesca Meneghellox, FilippoCampagnarox, Roee Diamantxz, Paolo Casari and Michele Zorzi, 2016. Design and Evaluation of a Low-Cost Acoustic Chamber, for Underwater Networking Experiments, *WUWNet*'16, Shanghai, China.

[5] Jon M. Collisa, William L. Siegmann, Michael D. Collins, Harry J. Simpson and Raymond J. Soukup, 2007. *J. Acoust. Soc. Am.*, **122**(4), 1987-1993.

[6] M.A. Biot, 1955. Theory of elasticity and consolidation for a porous anisotropic solid, *J. App. Phys.*, **26**(2), 182-185.

[7] M.A. Biot, 1956. General solutions of the equations of elasticity and consolidation for a porous material, *J. App. Mech.*, **78**, 91-96.

[8] M.A. Biot, 1956. Theory of propagation of elastic waves in a fluid saturated porous solid. I. Low frequency range, *J. Acoust. Soc. Am.*, **28**(2), 168-78.

[9] M.A. Biot, 1956. Theory of deformation of a porous viscoelastic anisotropic solid, *J. App. Phys.*, **27**(5), 459-467.

[10] M.A. Biot, 1962. Mechanics of deformation and acoustic propagation in porous media, *J. App. Phys.*, **33**(4), 1482-1498.

[11] Comsol Multiphysics 5.2, Pressure Acoustics module, Manual.

INFORMATION FOR AUTHORS

ARTICLES

The Journal of Acoustical Society of India (JASI) is a refereed publication published quarterly by the Acoustical Society of India (ASI). JASI includes refereed articles, technical notes, letters-to-the-editor, book review and announcements of general interest to readers.

Articles may be theoretical or experimental in nature. But those which combine theoretical and experimental approaches to solve acoustics problems are particularly welcome. Technical notes, letters-to-the-editor and announcements may also be submitted. Articles must not have been published previously in other engineering or scientific journals. Articles in the following are particularly encouraged: applied acoustics, acoustical materials, active noise & vibration control, bioacoustics, communication acoustics including speech, computational acoustics, electro-acoustics and audio engineering, environmental acoustics, musical acoustics, non-linear acoustics, noise, physical acoustics, physiological and psychological acoustics, quieter technologies, room and building acoustics, structural acoustics and vibration, ultrasonics, underwater acoustics.

Authors whose articles are accepted for publication must transfer copyright of their articles to the ASI. This transfer involves publication only and does not in any way alter the author's traditional right regarding his/her articles.

PREPARATION OF MANUSCRIPTS

All manuscripts are refereed by at least two referees and are reviewed by the Publication Committee (all editors) before acceptance. Manuscripts of articles and technical notes should be submitted for review electronically to the Chief Editor by e-mail or by express mail on a disc. JASI maintains a high standard in the reviewing process and only accept papers of high quality. On acceptance, revised articles of all authors should be submitted to the Chief Editor by e-mail or by express mail.

Text of the manuscript should be double-spaced on A4 size paper, subdivided by main headings-typed in upper and lower case flush centre, with one line of space above and below and sub-headings within a section-typed in upper and lower case understood, flush left, followed by a period. Sub-sub headings should be italic. Articles should be written so that readers in different fields of acoustics can understand them easily. Manuscripts are only published if not normally exceeding twenty double-spaced text pages. If figures and illustrations are included then normally they should be restricted to no more than twelve-fifteen.

The first page of manuscripts should include on separate lines, the title of article, the names, of authors, affiliations and mailing addresses of authors in upper and lowers case. Do not include the author's title, position or degrees. Give an adequate post office address including pin or other postal code and the name of the city. An abstract of not more than 200 words should be included with each article. References should be numbered consecutively throughout the article with the number appearing as a superscript at the end of the sentence unless such placement causes ambiguity. The references should be grouped together, double spaced at the end of the article on a separate page. Footnotes are discouraged. Abbreviations and special terms must be defined if used.

EQUATIONS

Mathematical expressions should be typewritten as completely as possible. Equation should be numbered consecutively throughout the body of the article at the right hand margin in parentheses. Use letters and numbers for any equations in an appendix: Appendix A: (A1, (A2), etc. Equation numbers in the running text should be enclosed in parentheses, i.e., Eq. (1), Eqs. (1a) and (2a). Figures should be referred to as Fig. 1, Fig. 2, etc. Reference to table is in full: Table 1, Table 2, etc. Metric units should be used: the preferred from of metric unit is the System International (SI).

REFERENCES

The order and style of information differs slightly between periodical and book references and between published and unpublished references, depending on the available publication entries. A few examples are shown below.

Periodicals:

[1] S.R. Pride and M.W. Haartsen, 1996. Electroseismic wave properties, *J. Acoust. Soc. Am.*, **100** (3), 1301-1315.
[2] S.-H. Kim and I. Lee, 1996. Aeroelastic analysis of a flexible airfoil with free play non-linearity, *J. Sound Vib.*, **193** (4), 823-846.

Books:

[1] E.S. Skudzryk, 1968. *Simple and Comlex Vibratory Systems*, the Pennsylvania State University Press, London.
[2] E.H. Dowell, 1975. *Aeroelasticity of plates and shells*, Nordhoff, Leyden.

Others:

[1] J.N. Yang and A. Akbarpour, 1987. Technical Report NCEER-87-0007, Instantaneous Optimal Control Law For Tall Buildings Under Seismic Excitations.

SUMISSIONS

All materials from authors should be submitted in electronic form to the JASI Chief Editor: B. Chakraborty, CSIR - National Institute of Oceanography, Dona Paula, Goa-403 004, Tel: +91.832.2450.318, Fax: +91.832.2450.602,(e-mail: bishwajit@nio.org) For the item to be published in a given issue of a journal, the manuscript must reach the Chief Editor at least twelve week before the publication date.

SUMISSION OF ACCEPTED MANUSCRIPT

On acceptance, revised articles should be submitted in electronic form to the JASI Chief Editor (bishwajit@nio.org)